Reviewed Preprint
v1 • January 24, 2024
Not revised

Reviewed Preprint
v2 • August 14, 2026
Revised by authors

The bile acid receptor TGR5 is a modulator of bone marrow adipose tissue and the hematopoietic niche

Alejandro Alonso-Calleja[1,2,*], Alessia Perino[2,*], Frédérica Schyrr[1,*], Silvia Ferreira Lopes[1], Vasiliki Delitsikou[2], Antoine Jalil[2], Ulrike Kettenberger[3], Maria Chiara Galavotti[1], Angela Martins[1], Charles Bataclan[1], Dominique P Pioletti[3], Kristina Schoonjans[2,†], Olaia Naveiras[1,4,†]

[1]Laboratory of Regenerative Hematopoiesis, Department of Biomedical Sciences, University of Lausanne, Lausanne, Switzerland • [2]Laboratory of Metabolic Signaling, Institute of Bioengineering, Ecole Polytechnique Fédérale de Lausanne, Lausanne, Switzerland • [3]Laboratory of Biomechanical Orthopedics, Ecole Polytechnique Fédérale de Lausanne, Lausanne, Switzerland • [4]Hematology Service, Departments of Oncology and Laboratory Medicine, Lausanne University Hospital (CHUV) and University of Lausanne (UNIL), Lausanne, Switzerland

For correspondence: olaia.naveiras@unil.ch

[*] These authors contributed equally and share first co-authorship.

[†] These authors co-directed the work and share corresponding authorship

Competing interests: No competing interests declared

Funding: See page 29

Reviewing editor: Owen J Tamplin, University of Wisconsin-Madison, United States

eLife Assessment

This study provides **valuable** insights into the role of the bile acid receptor TGR5 in regulating bone marrow adipose tissue. This revised manuscript has additional characterization of TGR5 expression in hematopoietic and stromal populations, and phenotypic differences observed between sexes, during aging, and under high-fat diet conditions. Although the scope of the study has expanded, the mechanism of how TGR5 in the microenvironment regulates hematopoietic recovery is still **incomplete**.

https://doi.org/10.7554/eLife.93124.2.sa3

Abstract

The gut is an emerging regulator of bone marrow (BM) hematopoiesis, with several signaling molecules involved in this communication. Among them, bile acids (BAs) act as a relay between the microbiota and the rest of the body through the activation of specific receptors, including Takeda G protein-coupled receptor 5 (TGR5). TGR5 has potent regulatory effects in immune cells, but its role in the BM as a primary immune organ remains unknown. Here, we demonstrate that TGR5 is expressed in hematopoietic progenitors and BM stromal progenitors. TGR5 deficiency did not affect steady-state hematopoiesis but led to impaired short-term progenitor reconstitution and reduced regulated bone marrow adipose tissue (BMAT) in young male mice, but not in female mice. The reduction in BMAT was accompanied by an enrichment in BM adipocyte progenitors and was associated with enhanced hematopoietic recovery upon BM transplantation into *Tgr5*$^{-/-}$ recipients. Moreover, its reduction was associated with lower myeloid-to-lymphoid progenitor ratios in obese and in aged *Tgr5*$^{-/-}$ male mice, resembling more those of lean or young controls. Our results indicate that TGR5 is essential for maintaining a balanced BM microenvironment in a sex-dependent manner and open the possibility of modulating stromal hematopoietic support by acting on TGR5 signaling.

Impact statement

TGR5 loss-of-function reduced regulated bone marrow adipose tissue in male mice, without affecting that of females at homeostasis, and accelerated myeloid recovery upon bone marrow transplantation. These data highlight TGR5 as a new player in the bone marrow microenvironment.

Introduction

The bone, long considered merely a structural organ, is now seen as a highly dynamic tissue in which various processes, including hematopoiesis, bone remodeling, immunity and metabolism are tightly regulated[1–4]. These processes rely on specialized microenvironments, termed niches, that play a critical role in cell fate regulation[5], with the bone marrow adipose tissue (BMAT) being an emerging niche component[6–10]. The bone marrow (BM) niche regulates hematopoietic stem and progenitor cell (HSPC) quiescence, self-renewal and commitment towards differentiated cells thanks to a combination of soluble factors and cell-cell interactions[1,5,11,12]. Osteoblasts, adipocytes and endothelial cells form the BM niche along with a wide range of BM stromal cells (BMSCs)[1,13]. While the involvement of these specific cell types in regulating hematopoiesis is generally accepted, the extent and nature of their action is controversial, especially for cells that form part of the adipocytic lineage. Mature BM adipocytes were first described to have a predominantly negative effect on hematopoietic recovery post-myeloablation[6,14,15]. Subsequent studies showing a positive effect of the BM adipocyte lineage on hematopoietic recovery called these results into question[7,16,17]. Recent work has uncovered a more nuanced role of non-lipidated BM adipogenic precursors in the control of bone homeostasis[8,9] and in favoring hematopoietic recovery upon irradiation[10,18,19]. As for other adipose depots, BMAT is plastic and can be remodeled upon injury and dietary or pharmacological stimulation[15,20–24].

Bone and BM homeostasis are influenced by extramedullary mechanisms, including the incompletely understood gut-BM cross-talk[25–28]. Communication between the gut and distant organs can be mediated by different signaling molecules, including bile acids (BAs), which are metabolites derived from the liver and subsequently modified by the gut microbiome into secondary BAs[29]. These BAs have emerged as powerful signaling molecules that modulate whole-body metabolism[30–32] through the activation of receptors such as the G protein-coupled receptor Takeda G protein-coupled receptor 5 (TGR5)[30]. BA-TGR5 signaling has been studied in a multitude of organs[31,32], and profoundly affects adipose tissue physiology through several mechanisms, ranging from beiging[33,34] and suppression of chronic inflammation in resident macrophages of the white adipose tissue (WAT)[35], to stimulation of fat oxidation in brown adipose tissue (BAT)[36–38]. In addition, TGR5 expression was observed in human BMSC-derived adipocytes[34], but the effect of TGR5 on BMAT and thus on BM function remains unknown. Previous reports have shown that BAs impact fetal and adult hematopoiesis acting as chemical chaperones[39–41] and, more recently, through direct interaction with myeloid precursors via the vitamin D receptor[42]. However, the effects at the level of the most studied membrane BA receptor TGR5, remain to be unraveled.

Here, we show that the loss of TGR5 does not affect BMAT volume in young female mice at homeostasis but markedly decreases BMAT in young and 1-year-old male mice on a standard chow-diet (CD), as well as in male mice fed a high-fat-diet (HFD). Concomitantly, we observe an increased representation of immunophenotypically-defined adipocyte-progenitor cells (APCs)[15] in the BM stroma and a hastened hematopoietic recovery upon BM transplantation. Notably, this enhanced recovery is determined by the recipient's genotype rather than the transplanted hematopoietic cells. These findings highlight TGR5 as a sex-specific regulator of BM microenvironment dynamics and a potential druggable target for modulating hematopoietic-stromal interactions.

Results

TGR5 is expressed in progenitors and differentiated hematopoietic populations

We initially aimed to define the presence of TGR5 in primitive and differentiated hematopoietic populations. For this, we used a GFP reporter mouse model driven by the *Tgr5* promoter (TGR5:GFP)[43]. Flow cytometry analysis of hematopoietic populations showed consistent GFP signal throughout the main hematopoietic stem and progenitor (HSPC) populations in the adult mouse

BM, with significant levels of GFP positivity in the lineage negative (Lin^-), c-Kit^+, $Sca1^+$ cells (LKS), a population highly enriched in murine hematopoietic stem and multipotent progenitor cells (Figure 1A, B).

We detected comparable frequencies of GFP^+ cells in populations downstream of the LKS gate, namely hematopoietic stem cells (HSC) and multipotent progenitors (MPP) (Figure 1C). Similar frequencies were observed in myeloid progenitors, with no marked differences between the different subpopulations, namely granulocyte-monocyte progenitors (GMP), common myeloid progenitors (CMP) and megakaryocyte-erythrocyte progenitors (MEP) (Figure 1C), as well as in megakaryocyte progenitors (MkProgs) (Figure 1D and Figure 1-figure supplement 1A). Regarding erythropoiesis[44], we observed a decreasing proportion of GFP-positive cells as cells matured (Figure 1E and Figure 1-figure supplement 1B). Analysis of fully differentiated hematopoietic populations in peripheral blood showed that TGR5 is predominantly expressed in myeloid lineage cells, with lower expression in lymphocytes (Figure 1F and Figure 1-figure supplement 2A). GFP was detected by immunohistochemistry in the BM (Figure 1G), spleen (Figure 1-figure supplement 2B) and, sparsely, in thymus (Figure 1-figure supplement 2C), confirming the expression of TGR5 in different immune organs. Taken together, these findings indicate that TGR5 is present throughout HSPC populations and is mostly restricted to the myeloid lineage upon differentiation.

TGR5 is not essential for steady-state hematopoiesis nor cell-autonomous hematopoietic stem cell function but regulates short-term BM repopulation capacity

We next hypothesized a role for TGR5 in hematopoietic progenitors and aimed to define the impact of TGR5 loss-of-function in hematopoiesis. Flow cytometry analysis of the BM of young male germline TGR5 knock-out ($Tgr5^{-/-}$) mice showed no marked alterations in the percentage (Figure 2A) or absolute number (Figure 2B) of HSPC populations compared to their controls ($Tgr5^{+/+}$). Functionally, we could not detect differences in hematopoietic colony-forming unit (CFU) potential, and thus functional blood cell progenitors, between $Tgr5^{-/-}$male mice and their $Tgr5^{+/+}$ counterparts (Figure 2-figure supplement 1A). Although we observed a nearly 20% increase in the average number of total $CD45^+$ cells per hindlimb collected from $Tgr5^{-/-}$ male mice (Figure 2C), this did not result in an increase in CFUs per hindlimb (Figure 2-figure supplement 1B). Complete blood counts (CBC) of peripheral blood showed a modest decrease in eosinophils with no change in other white blood cell populations in $Tgr5^{-/-}$ male mice (Figure 2D, E). Additionally, we observed a moderate increase in the number of red blood cells, but no change in hemoglobin or platelet levels, in $Tgr5^{-/-}$ male mice (Figure 2F-H). This result differs from recently published work, which showed a modest gain in circulating platelets in $Tgr5^{-/-}$ mice[45]. Female mice behaved similarly, not showing differences in BM HSPC populations (Figure 2-figure supplement 1C). CBC of young female mice showed no differences in circulating cells between both genotypes, except for monocytes, in which a moderate decrease was observed in the $Tgr5^{-/-}$ mice (Figure 2-figure supplement 1D-H). Taken together, these results indicate that TGR5 is not required for normal hematopoietic progenitor function in steady-state hematopoiesis, in neither male nor female young adult mice.

In the next step, we aimed to define the cell-autonomous effects of a TGR5 germline deletion in hematopoietic stem and progenitor cells in response to stress. To investigate this, we examined the hematopoietic repopulating capacity of $Tgr5^{-/-}$ and $Tgr5^{+/+}$ total BM cells when co-transplanted with competitor CD45.1/.2 BM into lethally irradiated wild-type recipients (CD45.1) (Figure 2I). Upon primary transplantation, $Tgr5^{-/-}$ donor cells showed an average 23% reduction in hematopoietic short-term repopulating capacity as compared to $Tgr5^{+/+}$ BM cells, the latter approaching the expected 50% average reconstitution capacity in the competitive transplant assay (47% for $Tgr5^{+/+}$ BM donors reduced to 36% average for $Tgr5^{-/-}$, p = 0.0169, Figure 2J, left panel). The blunted short-term hematopoietic repopulating capacity for $Tgr5^{-/-}$donor BM cells was rescued at later timepoints, when hematopoietic stem- and not progenitor- cells are responsible for reconstitution (Figure 2J, right panel). Further, we did not observe any difference in

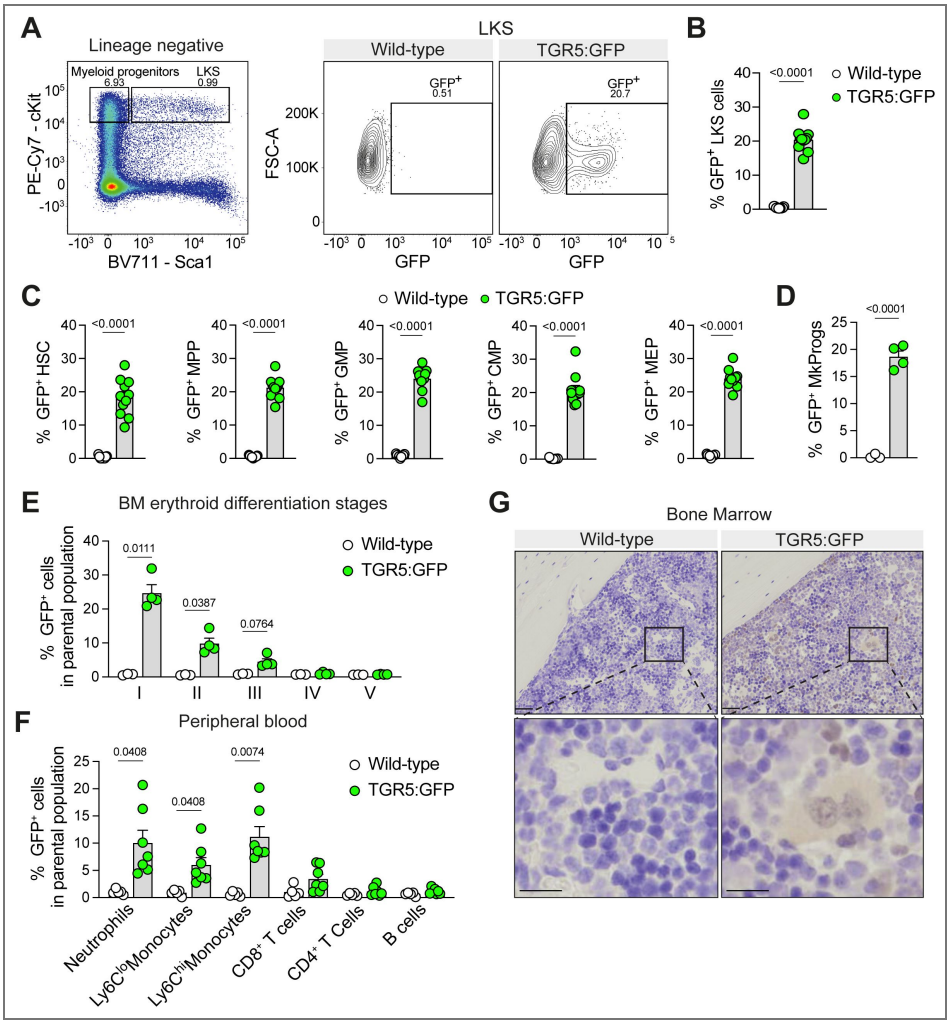

Figure 1. TGR5 is expressed in BM hematopoietic stem, in progenitor cells (HSPCs) and in differentiated myeloid populations.

(**A**) Representative flow cytometry gating strategy used to identify HSPCs and GFP positivity in TGR5:GFP mice and their wild-type controls. (**B**) Frequency of GFP$^+$ cells in the Lineage$^-$cKit+Sca1$^+$ (LKS) population in the BM of 8- to 12-week-old TGR5:GFP male mice and their controls (n=9 for wild-type mice, n=11 for TGR5:GFP mice). (**C**) Frequency of GFP$^+$ cells in hematopoietic stem cells (HSCs), multipotent progenitors (MPPs), granulocyte-monocyte progenitors (GMPs), common myeloid progenitors (CMPs) and megakaryocyte-erythrocyte progenitors (MEPs) in the BM of the mice described in **B**. (**D**) Frequency of GFP$^+$ cells in megakaryocyte progenitor (MkProgs) in the BM of the mice described in **B**. (**E**) Frequency of GFP$^+$ cells in the different stages of erythropoiesis in the BM of 8- to 12-week-old male TGR5:GFP mice and their wild-type controls (n=3 for wild-type mice, n=4 for TGR5:GFP mice); axis represents % GFP$^+$ cells within the parental population. (**F**) Frequency of GFP$^+$ cells in peripheral blood cell populations of 8- to 12-week-old male TGR5:GFP mice and their wild-type controls (n=5 for wild-type mice, n=7 for TGR5:GFP mice). (**G**) Immunodetection of GFP$^+$ cells by DAB IHC in BM of 8- to 12-week-old TGR5:GFP male mice (n=2 for wild-type mice, n=3 for TGR5:GFP mice). Scale bar: 50 μm in low magnification images, 20 μm in the corresponding digitally zoomed images. Results represent the mean ± s.e.m., n represents biologically independent replicates. Unpaired, two-tailed Student's t-test (**B**, **C**, **D**), multiple two-tailed Student's t-test with Holm-Sidak's multiple comparison correction (**E**, **F**) was used for statistical analysis. P values are indicated.

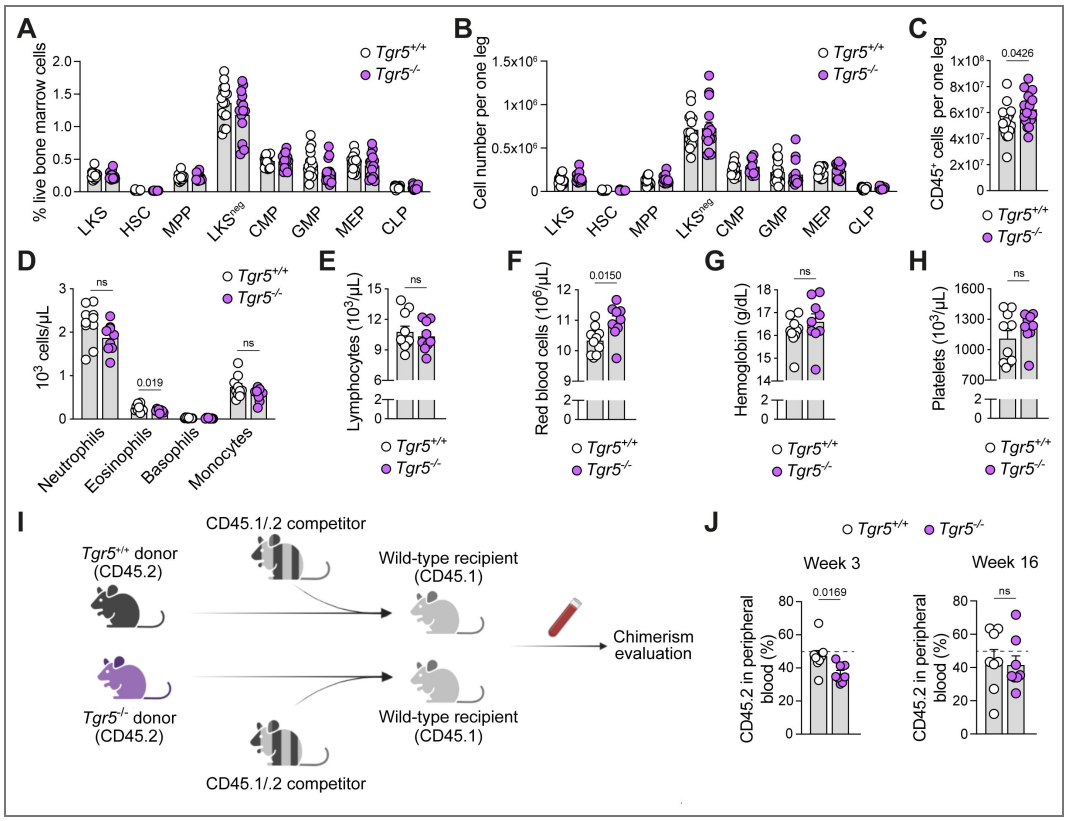

Figure 2. Loss of TGR5 does not impair steady state hematopoiesis but compromises hematopoietic progenitor function in stress hematopoiesis.

(**A**) Frequency of hematopoietic stem and progenitor (HSPC) populations in the BM of 8-to 12-week-old *Tgr5*$^{+/+}$ and *Tgr5*$^{-/-}$ male mice expressed as percentage of cells over total live cells acquired (n=16 for *Tgr5*$^{+/+}$ and n=15 for *Tgr5*$^{-/-}$ mice). (**B**) Total number of cells per one leg (hip, femur and tibia) for HSPC populations in the BM of the mice described in **A**. (**C**) Total number of CD45^{+} cells per one leg (hip, femur and tibia) of the mice described in **A**. (**D-H**) Complete blood counts in peripheral blood of 8- to 12-week-old *Tgr5*$^{+/+}$ (n=10) and *Tgr5*$^{-/-}$ (n=9) male mice; myeloid cells (**D**), lymphocytes (**E**), red blood cells (**F**), hemoglobin (**G**), and platelets (**H**). (**I**) Workflow depicting the primary competitive transplant setting. (**J**) Flow cytometry analysis of peripheral blood chimerism in primary transplantation recipients (n=8, 8- to 12-week-old *Tgr5*$^{+/+}$ and *Tgr5*$^{-/-}$ male donors transplanted into 2-3 CD45.1 recipient mice, treated as technical replicates per donor) at 3 (short-term progenitor readout) and 16 weeks (stem cell contribution readout) post-transplant. Axis represents % CD45.2 donor cells over the sum of CD45.2 donor and CD45.1/.2 competitor events. Dashed line refers to the expected contribution. Results represent the mean ± s.e.m., n represents biologically independent replicates unpaired, two-tailed Student's t-test (**C**, **D**, **F**, **J**) was used for statistical analysis. P values (exact value) are indicated, ns indicates non-significance.

repopulating capacity in the secondary or tertiary transplant in the wild-type donors (Figure 2-figure supplement 1I), with an overall balanced contribution of the lymphoid and myeloid lineage throughout (Figure 2-figure supplement 1J, K), which further indicates preserved hematopoietic stem cell function. Taken together, these findings indicate that *Tgr5*$^{-/-}$ BM cells exhibit a transient deficit in short-term repopulating progenitor capacity that is corrected over serial transplantation in wild-type recipients, with no detectable long-term impairment of hematopoietic stem cell function.

TGR5 regulates the BM microenvironment

Based on our findings that functional hematopoietic progenitors are quantitatively conserved at homeostasis and that the cell-autonomous effects on short-term hematopoietic progenitors disappear on serial transplantation (i.e., exposure to a wild-type BM niche), we hypothesized that an altered BM microenvironment in *Tgr5*$^{-/-}$ animals may account for this phenotype. In agreement with the literature[46], we found that young adult *Tgr5*$^{-/-}$ male mice display a decrease in bone volume fraction (BV/TV) and trabecular number (Tb.N.) with no changes in trabecular thickness (Tb.Th.) or separation (Tb.Sp.) at the distal femur (Figure 3A,B). In addition, no alterations in cortical parameters were found at the level of the femoral diaphysis (Figure 3-figure supplement 1A, B), as evaluated by micro-computed tomography (μCT). We could not detect any changes in bone microarchitecture in the spine at the level of L4 in young male *Tgr5*$^{-/-}$ mice (Figure 3-figure supplement 1C, D). These data suggest that the role of TGR5 on bone microarchitecture diverges based on skeletal location, which is in line with the recently described differential regulation of the axial and appendicular skeletons[47,48].

To further study the overall composition of the BM microenvironment, we used osmium tetroxide (OsO_4) contrast-enhanced μCT[49] to visualize total lipid content in the BM cavity as a readout for BMAT. The BMAT in the proximal tibia, also known as regulated BMAT (rBMAT), is regarded as the most dynamic and stimuli-responsive BMAT in opposition to that found in the distal tibia, which is enriched in the less responsive, constitutive BMAT (cBMAT)[50]. This analysis revealed a profound reduction in proximal tibia rBMAT in young adult *Tgr5*$^{-/-}$ male animals, as well as a less marked decrease in distal tibia cBMAT compared to age-matched controls (*Tgr5*$^{+/+}$) (Figure 3C, D). Young *Tgr5*$^{-/-}$ females showed a trend towards lower trabecular BV/TV in the appendicular skeleton (Figure 3E, F), a smaller cross-sectional area of the femoral diaphysis (Figure 3-figure supplement 1E-F) and no differences in L4 (Figure 3-figure supplement 1G-H). There was no difference in tibia BMAT between groups (Figure 3G,H), indicating that the effect of TGR5 deletion on BMAT in young mice is sexually dimorphic and is congruent with recent work pointing towards a differential regulation of BMAT in male and female mice[51].

We next sought to evaluate whether the decrease in rBMAT with a more preserved cBMAT was exclusive to the appendicular skeleton or was also present in axial structures in male mice. For this, we chose the caudal spine, as this segment of the vertebral column contains a gradient where rBMAT gives way to cBMAT in a proximal-to-distal manner[52]. μCT scanning of OsO_4-stained caudal spines showed this adipocytic gradient, so-called the yellow-to-red transition at the level of the second caudal vertebrae (CA2) in young male *Tgr5*$^{+/+}$ mice. Analogously to our findings for the rBMAT in tibia, *Tgr5*$^{-/-}$ male mice presented a marked decrease in BMAT at the level of CA2 (Figure 3-figure supplement 2A-C). Histological preparations of the same spine segments from an independent cohort further confirmed our μCT data (Figure 3-figure supplement 2D). Taken together, our data indicate that TGR5 regulates the composition of the BM microenvironment in a skeletal location- and sex- specific manner.

TGR5-dependent reduction of BMAT accrual and myeloid bias associated with age and obesity

As mice lose bone and accumulate BMAT with age[52], we evaluated the hindlimbs of 1-year-old *Tgr5*$^{-/-}$ male mice, expecting that the observed bone loss in young males would persist, as shown in previous work[46], and BMAT expansion may be blunted. Accordingly, 1-year-old *Tgr5*$^{-/-}$ male mice showed a decrease in mineralized tissue in the femoral metaphysis (Figure 4A, B) and, to a

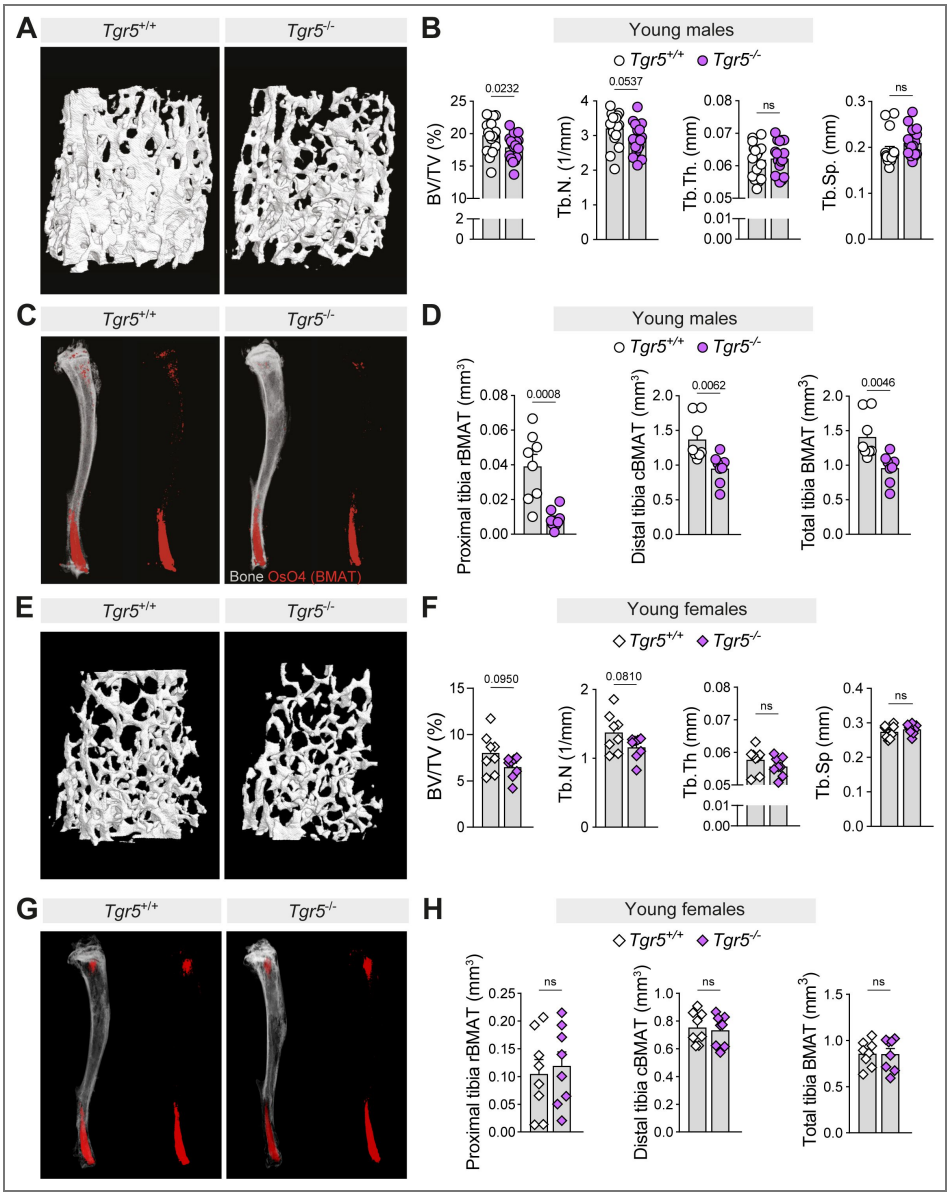

Figure 3. Loss of TGR5 alters the BM microenvironment in male but not in female mice.

(**A**) Representative native µCT-derived 3D reconstructions of the trabecular structure in the distal femoral metaphysis of 8- to 12-week-old *Tgr5*$^{+/+}$ and *Tgr5*$^{-/-}$ male mice. (**B**) µCT-derived bone morphometry measurements of the trabecular structure in the distal femoral metaphysis of 8- to 12-week-old *Tgr5*$^{+/+}$ and *Tgr5*$^{-/-}$ male mice (n=17 for both *Tgr5*$^{+/+}$ and *Tgr5*$^{-/-}$ mice); shown are bone volume/total volume (BV/TV), trabecular number (Tb.N.), trabecular thickness (Tb.Th.) and trabecular separation (Tb.Sp.). (**C**) Representative contrast-enhanced µCT-derived 3D reconstructions of osmium tetroxide (OsO_4)-stained BMAT in the tibias of 8- to 12-week-old *Tgr5*$^{+/+}$ and *Tgr5*$^{-/-}$ male mice. (**D**) Quantification of the OsO_4-stained bone marrow adipose tissue (BMAT) content in 8- to 12-week-old *Tgr5*$^{+/+}$ and *Tgr5*$^{-/-}$ male mice (n=8 for both *Tgr5*$^{+/+}$ and *Tgr5*$^{-/-}$ mice). OsO_4-stained regulated BMAT proximal of tibiofibular junction was classified as "proximal rBMAT"; OsO_4-stained constitutive BMAT distal of tibiofibular junction was classified as "distal cBMAT". (**E**) Representative native µCT-derived 3D reconstructions of the trabecular structure in the distal femoral metaphysis of 8-week-old *Tgr5*$^{+/+}$ and *Tgr5*$^{-/-}$ female mice. (**F**) µCT-derived bone morphometry measurements of the trabecular structure in the distal femoral metaphysis of 8-week-old *Tgr5*$^{+/+}$ and *Tgr5*$^{-/-}$ female mice (n=8 for both *Tgr5*$^{+/+}$ and *Tgr5*$^{-/-}$ mice); parameters shown analogously to **B**. (**G**) Representative contrast-enhanced µCT-derived 3D reconstructions of OsO_4-stained BMAT in the tibias of 8-week-old *Tgr5*$^{+/+}$ and *Tgr5*$^{-/-}$ female mice. (**H**) Quantification of the OsO_4-stained BMAT content in 8-week-old *Tgr5*$^{+/+}$ and *Tgr5*$^{-/-}$ female mice (n=8 for both *Tgr5*$^{+/+}$ and *Tgr5*$^{-/-}$ mice). Proximal and distal BMAT were defined as in **D**. Results represent the mean ± s.e.m., n represents biologically independent replicates. Unpaired, two-tailed Student's t-test **(B, D, F, H)** was used for statistical analysis. P values (exact value) are indicated, ns indicates no statistical significance.

milder extent, in the femoral diaphysis and L4 vertebral body (Figure 4-figure supplement 1A-D). Similarly, we observed a reduction in tibia BMAT compared to their age-matched controls (Figure 4C, D). As BMAT expansion has been linked to a myeloid bias in BM progenitors[53–55] and *Tgr5*$^{-/-}$ animals fail to expand this tissue upon aging, we hypothesized that the loss of TGR5 would blunt these changes. In agreement with our hypothesis, we found that the CMP/CLP ratio in 1-year-old *Tgr5*$^{-/-}$ male mice was significantly lower than that of their wild-type controls (Figure 4E, F).

Dietary intervention has also been shown to modulate bone microarchitecture and BMAT, with high-fat diet (HFD)-feeding decreasing mineralized tissue and robustly increasing marrow adiposity in general and rBMAT in particular[15,56,57]. To investigate if TGR5 modulates the BM niche upon this dietary intervention, we fed *Tgr5*$^{-/-}$ and *Tgr5*$^{+/+}$ male mice with an HFD for 12 weeks and evaluated hindlimbs as in 1-year-old animals. Compared to their wild-type controls, *Tgr5*$^{-/-}$ animals fed HFD showed a slightly more marked deterioration of their trabecular bone microarchitecture (Figure 5A, B) with minimal impact on cortical parameters (Figure 5-figure supplement 1A, B), and a marked decrease in rBMAT along with a more moderate decrease in cBMAT (Figure 5C, D). Moreover, and in line with the data gathered from the CD-fed 1-year-old mice, the CMP/CLP ratio in HFD-fed *Tgr5*$^{-/-}$ male mice was similar to that of our younger, CD-fed cohorts (Figure 5-figure supplement 1C).

Taken together, our findings indicate a mutual loss of trabecular bone and marrow adiposity in *Tgr5*$^{-/-}$ male mice. Specifically, loss of TGR5 decreased trabecular bone in the appendicular skeleton without affecting bone structure at the level of the axial skeleton, other than in older animals. Conversely, lack of TGR5 markedly reduced BMAT volume in both the appendicular and axial skeleton in male mice. The decrease in BMAT occurred fundamentally at the expense of rBMAT both at homeostasis and under aging- or HFD-induced expansion of BMAT, suggesting that TGR5 might be a key player in the regulation of this tissue.

Loss of TGR5 promotes adipocyte progenitor accumulation and accelerates hematopoietic recovery post-transplant

Given the changes in both BMAT and bone architecture, we hypothesized that BMSCs obtained from *Tgr5*$^{-/-}$ mice would present a defect in both adipocytic and osteoblastic differentiation. TGR5 was present in the stroma-enriched CD45^{-}Ter119^{-}CD31^{-} population as determined by GFP positivity in the TGR5:GFP reporter model (Figure 6A, B) albeit at lower levels than in HSPCs (Figure 1A-D). Contrary to our hypothesis, *Tgr5*$^{-/-}$ BMSCs differentiated more readily into adipocytes, as evidenced by Oil Red O staining (ORO) (Figure 6C, D and Figure 6-figure supplement 1A) and digital holographic microscopy (Figure 6E, F)[58]. Moreover, *Tgr5*$^{+/+}$ and *Tgr5*$^{-/-}$ BMSCs displayed comparable osteoblastic differentiation, evaluated by alkaline phosphatase staining (ALP) (Figure 6G) and calcium deposition, as evidenced by alizarin red staining (Figure 6H). Taken together, these data indicate that TGR5 deletion does not cause an intrinsic defect in *in vitro* BMSC differentiation.

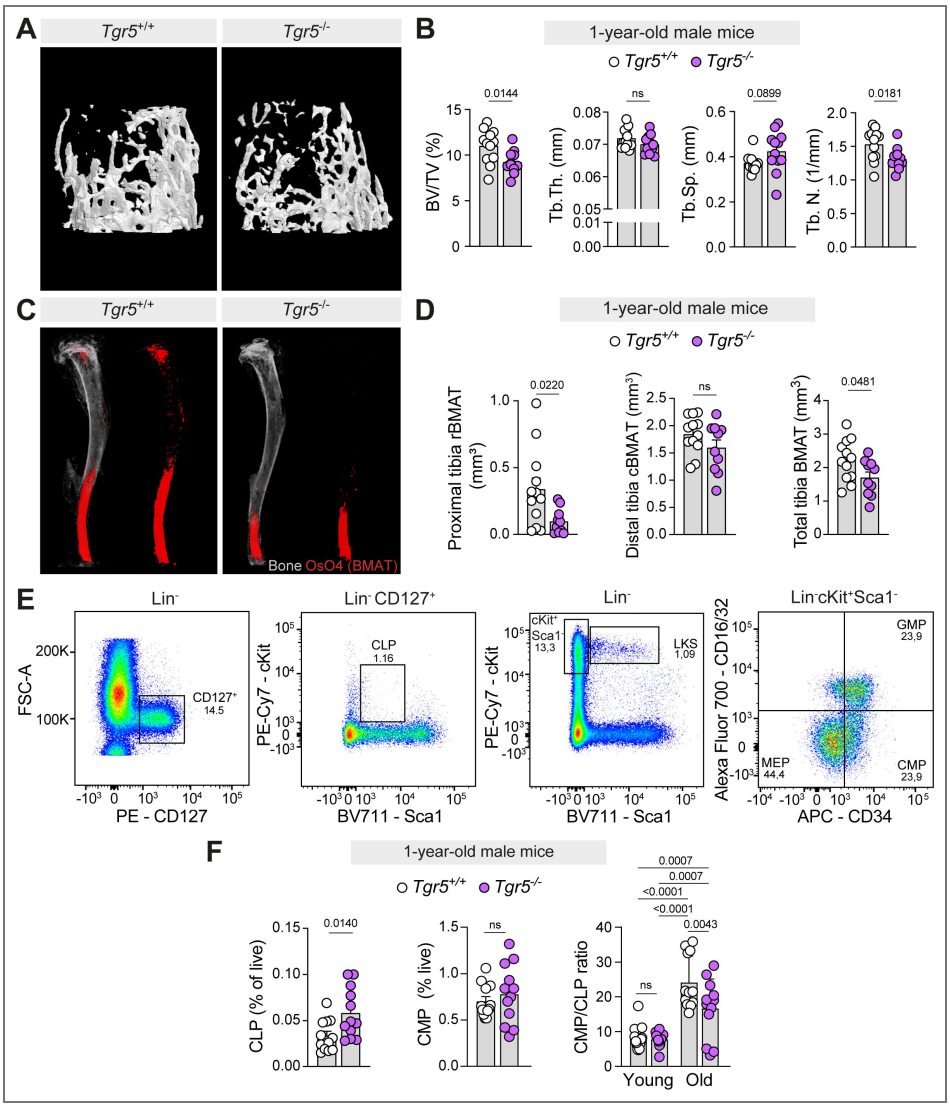

Figure 4. Loss of TGR5 alters the BM microenvironment and blunts BM HSPC myeloid bias in 1-year-old male mice.

(**A**) Representative native µCT-derived 3D reconstructions of the trabecular structure in the distal femoral metaphysis of 1-year-old *Tgr5*$^{+/+}$ and *Tgr5*$^{-/-}$ male mice. (**B**) µCT-derived bone morphometry measurements of the trabecular structure in the distal femoral metaphysis of 1-year-old *Tgr5*$^{+/+}$ and *Tgr5*$^{-/-}$ male mice (n=12 for both *Tgr5*$^{+/+}$ and *Tgr5*$^{-/-}$ mice); shown are bone volume/total volume (BV/TV), trabecular thickness (Tb.Th.), trabecular separation (Tb.Sp.) and trabecular number (Tb.N.). (**C**) Representative contrast-enhanced µCT-derived 3D reconstructions of osmium tetroxide (OsO_4)-stained bone marrow adipose tissue (BMAT) in the tibias of 1-year-old *Tgr5*$^{+/+}$ and *Tgr5*$^{-/-}$ male mice. (**D**) Quantification of the OsO_4-stained BMAT content 1-year-old *Tgr5*$^{+/+}$ and *Tgr5*$^{-/-}$ male mice (n=12 for *Tgr5*$^{+/+}$ and n=11 for *Tgr5*$^{-/-}$ mice). OsO_4-stained regulated BMAT proximal of tibiofibular junction was classified as "proximal rBMAT"; OsO_4-stained constitutive BMAT distal of tibiofibular junction was classified as "distal cBMAT". (**E**) Representative gating strategy for common myeloid progenitors (CMP) and common lymphoid progenitors (CLP). (**F**) Frequency of common lymphoid progenitors (CLP), common myeloid progenitors (CMP) and ratio of CMP-to-CLP cells in the BM of 8- to 12-week-old (calculated from the data presented in Figure 2A-B) and 1-year-old *Tgr5*$^{+/+}$ and *Tgr5*$^{-/-}$ male mice (n=12 for both *Tgr5*$^{+/+}$ and *Tgr5*$^{-/-}$ mice). Results represent the mean ± s.e.m., n represents biologically independent replicates. Unpaired, two-tailed Student's t-test (**B**, **D**, **F**) and 2-way ANOVA test with Holm-Sidak's multiple comparison correction (CMP/CLP ratio in **F**) were used for statistical analysis. Exact p-values are indicated; ns indicates non-significance.

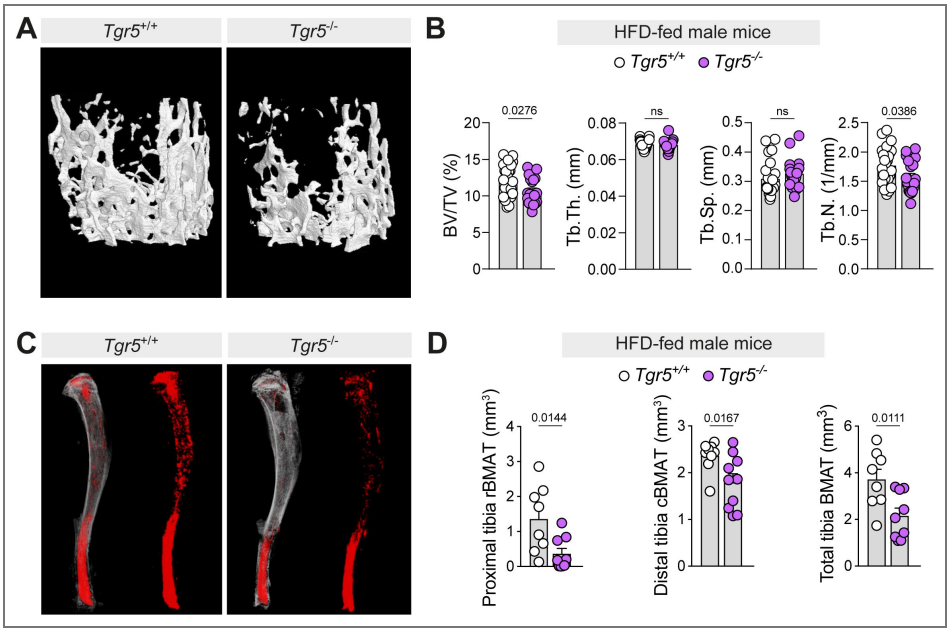

Figure 5. Loss of TGR5 alters the BM microenvironment in HFD-fed male mice.

(**A**) Representative native µCT-derived 3D reconstructions of the trabecular structure in the distal femoral metaphysis of *Tgr5*$^{+/+}$ and *Tgr5*$^{-/-}$ male mice fed with a high-fat diet (HFD) for 12 weeks. (**B**) µCT-derived bone morphometry measurements of the trabecular structure in the distal femoral metaphysis of HFD-fed *Tgr5*$^{+/+}$ and *Tgr5*$^{-/-}$ male mice (20-week-old at the end of the intervention, n=24 for *Tgr5*$^{+/+}$ and n=19 for *Tgr5*$^{-/-}$); shown are bone volume/total volume (BV/TV), trabecular thickness (Tb.Th.), trabecular separation (Tb.Sp.) and trabecular number (Tb.N.). (**C**) Representative contrast-enhanced µCT-derived 3D reconstructions of osmium tetroxide (OsO_4)-stained bone marrow adipose tissue (BMAT) in the tibias of *Tgr5*$^{+/+}$ and *Tgr5*$^{-/-}$ male mice fed with a HFD for 12 weeks. (**D**) Quantification of the OsO_4-stained BMAT content of mice *Tgr5*$^{+/+}$ and *Tgr5*$^{-/-}$ male mice fed with a HFD for 12 weeks (n=9 for *Tgr5*$^{+/+}$ and n=10 for *Tgr5*$^{-/-}$ mice). OsO_4-stained regulated BMAT proximal of tibiofibular junction was classified as "proximal rBMAT"; OsO_4-stained constitutive BMAT distal of tibiofibular junction was classified as "distal cBMAT". Results represent the mean ± s.e.m., n represents biologically independent replicates. Unpaired, two-tailed Student's t-test (**B**, **D**) was used for statistical analysis. Exact p-values are indicated; ns indicates non-significance.

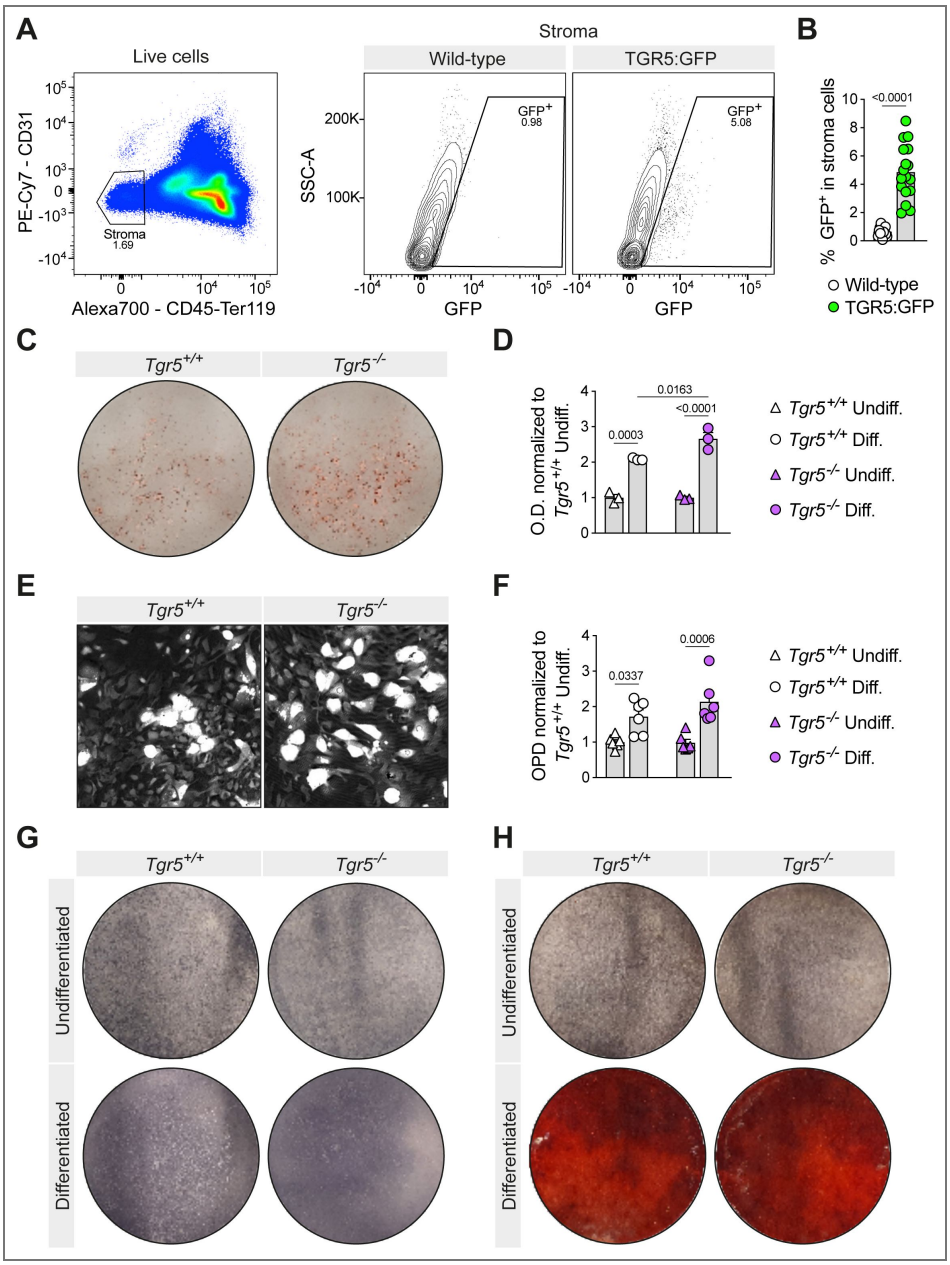

Figure 6. TGR5 is expressed in BM stroma, and its loss do not cause an intrinsic BMSC differentiation defect *in vitro*.

(**A**) Representative flow cytometry gating strategy used to identify the stroma-enriched CD45$^-$Ter119$^-$CD31$^-$ gate and the GFP of the cells contained in BM of TGR5:GFP mice. (**B**) Frequency of GFP$^+$ cells in the stroma-enriched population of 8- to 12-week-old male TGR5:GFP mice and their wild-type controls (n=15 for wild-type mice, n=17 for TGR5:GFP mice, axis represents % GFP$^+$ cells within the parental population). (**C,D**) Representative images (**C**) and spectrophotometric quantification (**D**) of Oil red O (ORO)-stained BMSCs after 7 days of adipocytic differentiation (n=3 for both *Tgr5*$^{+/+}$ and *Tgr5*$^{-/-}$ mice). (**E,F**) Digital holographic microscopy imaging of BMSCs after 7 days of adipocytic differentiation showing representative images; lipid inclusions appear as bright white areas in this technique (**E**), and optical path difference (OPD) quantification, indicative of the degree of lipidation (**F**). (**G,H**) Alkaline phosphatase (ALP) (**G**) and alizarin red (AR) (**H**) performed after ALP stains of BMSCs after 7 days of osteoblastic differentiation. All cells were obtained from 8- to 12-week-old *Tgr5*$^{+/+}$ and *Tgr5*$^{-/-}$ male mice. Results represent the mean ± s.e.m., n represents biologically independent replicates. Unpaired, two-tailed Students t-test (**B**) and one-way ANOVA with Tukey's multiple test correction (**D**) or Holm-Šídák's multiple test correction (**F**) were used for statistical analysis. P values (exact value) are indicated.

Recent reports have revealed that lipodystrophy or specific ablation of pre-adipocytic populations in the BM leads to massive trabecular bone invasion of the medullary cavity, indicating that these populations negatively regulate the mineralized compartment of the BM microenvironment[6,8–10,46,59–61]. We hypothesized that our findings in *Tgr5*$^{-/-}$ mice could be explained by an *in vivo* blockage of lipidation for specific adipocyte progenitors, namely APCs, or an increased rate of delipidation of mature adipocytes[19] that is reversed upon forced induction of *in vitro* adipocytic differentiation. In order to assess this, we analyzed the BM stroma based on the expression of Sca1 and CD24 for APC quantification[15]. In agreement with our hypothesis, we found an increase in the proportion of immunophenotypic APCs (CD45^{-}Ter119^{-}CD31^{-}Sca1^{+}CD24^{-}) in the stroma of *Tgr5*$^{-/-}$ mice (Figure 7A). Finally, we observed an alteration in the clonogenic capacity of BMSCs, evidenced by an increase in fibroblast colony-forming units (CFU-F) in *Tgr5*$^{-/-}$ BM compared to wild-type controls (Figure 7B), which agrees with a shift towards less differentiated BM stromal populations in *Tgr5*$^{-/-}$ animals. Taken together, our findings indicate that TGR5 loss-of-function perturbs the equilibrium of stromal populations within the marrow cavity and suggest that TGR5 signaling is necessary for BM pre-adipocytes to form or retain lipid droplets.

Given the enrichment of APCs in the stroma of *Tgr5*$^{-/-}$mice, we next investigated the impact of the associated BM microenvironment alterations in stress hematopoiesis. Lipidated BM adipocytes have been described as negative regulators of hematopoietic recovery[6], and recent work has shown that non-lipidated adipocytic precursors improve hematopoietic recovery[18]. Considering this, we hypothesized that the shift towards more non-lipidated progenitors in the BM microenvironment of *Tgr5*$^{-/-}$ mice would correlate with an improved early hematopoietic recovery upon irradiation and transplantation.

To assess this, we generated inverse chimeras in a lethal irradiation rescue set-up (Figure 7C) and evaluated early hematopoietic recovery using CBCs as a direct readout of the functionality of the hematopoietic system for the first 4 weeks post-irradiation. We observed a trend towards lower mortality post-transplant in the *Tgr5*$^{-/-}$recipients (Figure 7D) and faster hematopoietic recovery in *Tgr5*$^{-/-}$ recipients upon lethal irradiation and transplantation with wild-type donor cells. *Tgr5*$^{-/-}$recipients recovered their platelet levels faster than the *Tgr5*$^{+/+}$recipients, showing values consistently above 200.000/µL one week sooner (Figure 7E); platelet levels below this threshold are considered a risk factor for bleeding events[62,63]. The recovery was also faster for white blood cells (WBCs) (Figure 7F) without a clear predominance of any cell type as shown for neutrophils (Figure 7G), monocytes (Figure 7H) or lymphocytes (Figure 7I). We observed no major differences in the recovery of red blood cells (RBCs) (Figure 7J). Taken together, our findings suggest that the loss of TGR5 leads to a BM stroma composition enriched in non-lipidated BMSC progenitors with conserved CFU-F potential that are beneficial for early hematopoietic recovery in a context of stress hematopoiesis.

Discussion

In the current study, we aimed to investigate the role of TGR5 on BM homeostasis. In contrast to recent work based on RNA expression data[64], flow cytometry analysis using TGR5:GFP reporter mice demonstrated that TGR5 is present in HSPCs, suggesting a more universal role of TGR5 in stem cell homeostasis[65].

Consistent with recently published work reporting TGR5 expression in platelets[45,66]., more differentiated populations, such as megakaryocytes, were also positive for GFP, In contrast, we did not observe an increase in circulating platelets in *Tgr5*$^{-/-}$ mice at baseline, contrary to a previous study[45], which may be attributable to differences in local animal facility conditions, as it has been shown for microbiome-dependent phenotypes[67,68]. We showed that, in young male mice, TGR5 loss-of-function leads to a relative enrichment of adipocytic precursors in the BM and a simultaneous loss of BMAT, suggesting that TGR5 is necessary for the *in vivo* maturation of BM adipocytes. The latter point was further confirmed by the blunting of BMAT expansion in both 1-year-old and HFD-fed *Tgr5*$^{-/-}$male mice. Further, both these conditions showed diminished increase in BM myeloid-lymphoid progenitor ratios for *Tgr5*$^{-/-}$ male mice, which is in line with the

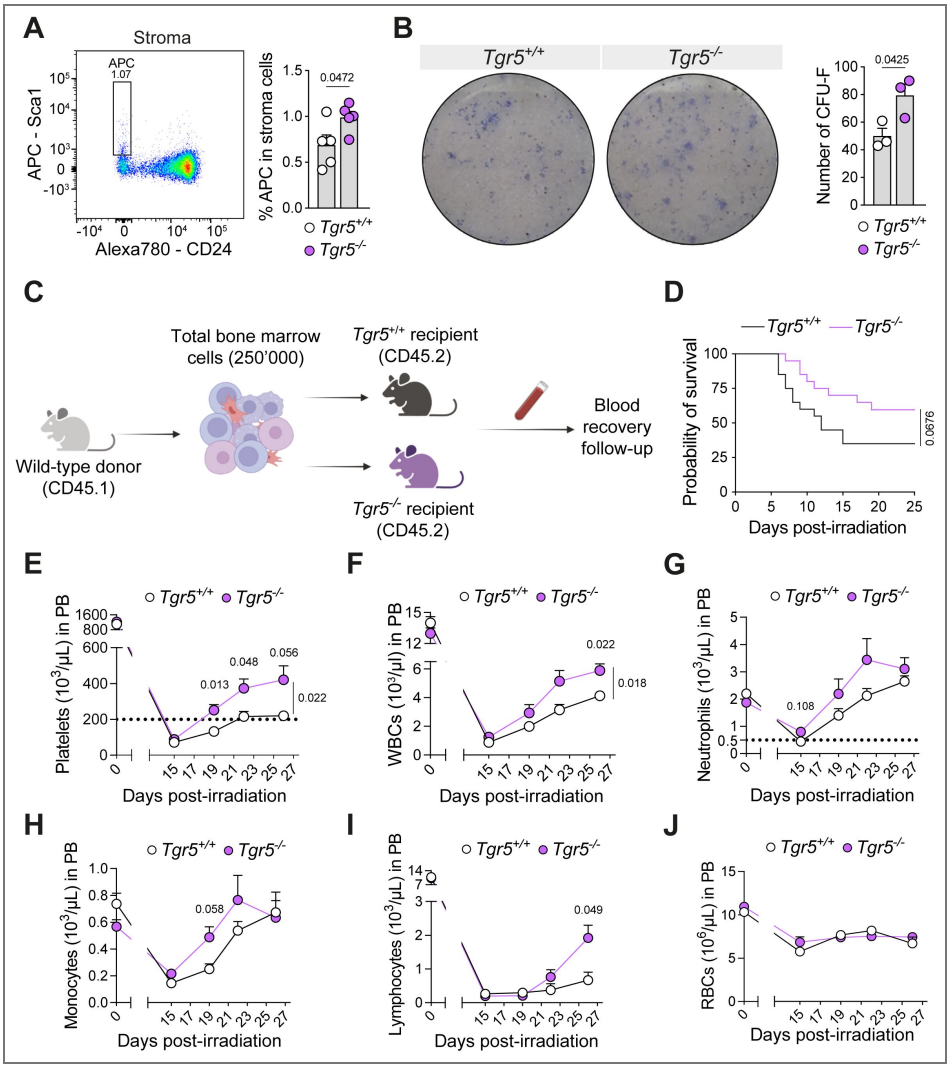

Figure 7. Loss of TGR5 leads to accumulation of adipocyte progenitors and hastens hematopoietic recovery upon irradiation and BM transplantation.

(**A**) Left: representative flow cytometry gating strategy for adipocyte progenitor cells (APC) in the BM stroma gate. Right: percentage of adipocyte progenitor cells (APC) in the $CD45^{-}Ter119^{-}CD31^{-}$ BM stromal gate (n=5 for both $Tgr5^{+/+}$ and $Tgr5^{-/-}$ mice). (**B**) Left: Representative images for fibroblast colony-forming unit (CFU-F) assay. Right: number of CFU-F obtained from 1 million total BM cells (n=3 both for $Tgr5^{+/+}$ and $Tgr5^{-/-}$ mice). Cells were obtained from 8- to 12-week-old male mice. (**C**) Schematic depiction of the inverse chimera transplantation setup. (**D**) Survival of BM transplant recipients (n=20 for both $Tgr5^{+/+}$ and $Tgr5^{-/-}$ at D0, 8- to 12-week-old male mice in 2 independent experiments). (**E-J**) Peripheral blood recovery evaluated longitudinally by complete blood counts for platelets (**E**), white blood cells (WBC) (**F**), neutrophils (**G**), monocytes (**H**), lymphocytes (**I**) and red blood cells (RBCs) (**J**) (n=7 for $Tgr5^{+/+}$ and n=12 $Tgr5^{-/-}$ 8- to 12-week-old male recipient mice). Results represent the mean ± s.e.m., n represents biologically independent replicates. Unpaired, two-tailed Student's t-test (**A, B**), Mantel-Cox's test (**D**) and two-way ANOVA with Holm-Šídák's multiple comparison correction (**E-J**) were used for statistical analysis. For **D**, baseline values (Day 0) were not considered for the analysis of the recovery. P values (exact value) are indicated.

relationship of BMAT expansion and myeloid skewing[69]. Young *Tgr5*$^{-/-}$ female mice, however, showed no changes in their BMAT, indicating that the effect of TGR5 on BMAT is sexually dimorphic at homeostasis, in line with recent reports[51].

BMAT and the BM adipocyte differentiation axis are gaining attention as a fundamental component of bone and blood physiology, with several recent studies focusing on the BM stroma population as a key player in the maintenance of the balance between bone and BM space[10,70]. Ablation of the BM adipocyte precursor population leads to massive accumulation of bone in the medullary cavity[6,9,16,60,63] which in turn reduces the volume available for hematopoietic tissue. In agreement with this model, we observe that *Tgr5*$^{-/-}$male mice display an increase in adipocytic precursors, a decrease in bone, and an expansion of CD45^{+} cells in the BM.

Similar to peripheral adipose depots, BMAT has been described as a highly dynamic tissue that responds to dietary changes, yet has distinct characteristics compared to extramedullary fat, not fully overlapping in its physiology with white or brown adipose tissues[71,72]. For instance, both nutrient deprivation (e.g. caloric restriction and anorexia) and excess (e.g. HFD feeding) result in BMAT expansion[57,73–75]. Although counterintuitive, this nutrient-mediated control of BMAT ensures energy conservation in BM to support the energy-consuming process of hematopoiesis and bone remodeling[76,77]. Another difference between BMAT and peripheral adipose tissues is the absence of HFD-induced pro-inflammatory response in the BMAT compared with the latter[57]. While the role of TGR5 in extramedullary adipose tissues has been extensively studied, and shown to be important for beige remodeling[33,34], lipolysis[34], and protection against diet-induced immune infiltration of the WAT[32,35], the effects of an activated TGR5 signaling pathway in BMAT and its impact on hematopoiesis is unknown. Elucidating where in the BM adipocyte differentiation axis, and how, TGR5 regulates BMAT requires further research.

Finally, we found that young *Tgr5*$^{-/-}$ male mice receiving BM transplantation after lethal irradiation recover faster than their *Tgr5*$^{+/+}$ counterparts in a setting of stress hematopoiesis. It is important to note that these experiments were carried out in a period during which our irradiated animals suffered from *swollen muzzles syndrome*, associating higher mortality than expected in the early post-transplant period, before hematopoietic toxicity is expected[78]. Therefore, our results should be interpreted within this specific context. While this condition is a limitation of the study, it also carries clinical relevance, as most transplant patients experience at least one episode of febrile neutropenia, often due to a severe infection arising from intestinal bacterial translocation or catheter entry sites[79,80]. While further studies are warranted to clarify how TGR5 influences transplant efficiency in infection-free settings, our findings clearly indicate a role for this receptor in the regulation of BMAT. Previous work has shown that *Tgr5* transcript levels increase during *in vitro* differentiation of human BMSCs to adipocytes[34,81]. Recently, it has been demonstrated that BMAT adipocytes can revert to non-lipidated precursors[19]. This plasticity may be relevant to interpreting our findings, as the BMAT phenotype observed in *Tgr5*$^{-/-}$ male mice could result from an accumulation of hematopoietic-supportive adipocyte precursors[18], a decrease in hematopoietic-quiescence inducing lipidated adipocytes[6], or a combination of both.

In addition to the role of TGR5, prior studies have linked BAs and transplantation outcomes. Of note, the BA ursodeoxycholic acid (UDCA) is routinely used in clinics in the context of BM transplantation, where supplementation with UDCA has been shown to reduce post-transplant complications and improve overall survival[82]. Available reports have attributed these benefits to the unique feature of the tauro-conjugated form of UDCA (TUDCA) as a chemical chaperone, improving protein folding in fetal liver HSCs[40] or after acute BM insult[41]. In addition, UDCA and TUDCA are hydrophilic BAs, and part of their beneficial effects could be a consequence of changes in the hydrophobicity of the BA pool[83,84]. BAs signal through dedicated BA receptors, but the receptor-mediated signaling of UDCA and TUDCA remains yet unclear. Although some studies proposed UDCA as a TGR5 agonist[85–88], effects occur mainly at supra-physiological doses of UDCA. In addition, the EC_{50} of UDCA for TGR5 is more than 60 times higher than that of the strongest endogenous TGR5 agonist, lithocholic acid (LCA)[89], indicating that UDCA is a poor TGR5 agonist. Based on this notion, it will be interesting to investigate whether, in this context, the benefits of UDCA upon stress hematopoiesis result from the inability to activate TGR5 signaling in the BMAT.

Novel therapeutic strategies could be envisioned in the future to pharmacologically mimic TGR5 inhibition in the BMAT. Although several selective TGR5 agonists have been developed, only a few TGR5 antagonists have been discovered, namely triamterene[90], SBI-115[91] and SBI-364[92]. However, these compounds have only been used *in vitro,* and additional *in vivo* research and optimization will be required to, transiently, pharmacologically block TGR5 in the BM upon transplantation or other conditions linked to stress hematopoiesis, in which a fast production of mature blood cells is required. Our results indicate that, although the exact mechanism remains to be clarified, deletion of TGR5 modulates the BM adipocyte lineage and suggest that strategies aimed at blocking the activity of this receptor might be therapeutically attractive.

Materials and methods

Mouse studies and ethical approval

Experiments were carried out in accordance with the Swiss law and with approval of the cantonal authorities (Service Vétérinaire de l'Etat de Vaud, authorization nos. 2990, 2990.1, 2990.2 and 3740).

Generation of mouse models and tissue collection

To evaluate the expression of TGR5, we used a transgenic mouse reporter model (TGR5:GFP), that co-expresses human TGR5 and the enhanced green fluorescent protein (GFP) linked by the foot-and-mouth disease virus (*F2a*) cleaving peptide sequence under the control of the endogenous *Tgr5* mouse promoter[43,93]. Mice in these groups were bred in-house at the EPFL facility as offspring of homozygous parents (not littermates) and age-matched as close as possible.

Mice were housed with ad libitum access to water and food and kept under a 12-h dark/12-h light cycle with a temperature of 22 °C ± 1 °C and a humidity of 60% ± 20%. 8- to 12-week-old male mice fed chow diet (CD, SAFE 150) were used for all experiments. 7- to 9-week-old female and 1-year-old male mice fed, both fed CD (SAFE 150) were used where indicated. For the HFD experiment, 8-week-old male mice were fed HFD (Research Diets D12492) for 12 weeks. The whole-body TGR5 knock-out mouse model ($Tgr5^{-/-}$) has been previously described[94]. Mice in these groups were bred in-house at the EPFL facility as offspring of homozygous parents (not littermates) and age-matched as close as possible.

C57BL/6J (CD45.2) and C57BL/6J Ly5.1 (CD45.1) mice were bred in-house at the EPFL facility. Double congenic mice (CD45.1/.2) were bred in-house, by F1s from the crossing of CD45.2 and CD45.1 mice.

BM transplantation

For transplantation assays, recipient mice were irradiated (lethal x-ray irradiation 8.5 Gy, split in two 4.25 Gy doses 4 h apart using an RS-2000 X-ray irradiator (RAD SOURCE)). Transplanted cells (total BM), obtained by crushing the hindlimb bones in a mortar and pestle, were administered the day following irradiation via tail-vein injection. For two weeks after lethal irradiation, mice were provided with paracetamol in drinking water (500 mg Dafalgan in 250 ml water). No antibiotics were provided in drinking water. For the primary competitive transplant setting, 300.000 total BM cells of each the CD45.2 donor ($Tgr5^{-/-}$ or $Tgr5^{+/+}$) and the CD45.1/.2 competitor were co-administered. For the secondary and tertiary transplant, 4 million cells were collected from the primary donor and transplanted into the recipient. For the inverse chimera experiments where the CD45.2 mice were the recipients ($Tgr5^{-/-}$ or $Tgr5^{+/+}$), 250.000 CD45.1 total BM cells were administered.

Blood collection for the experiments described in this work was performed at noon. Blood was obtained from the tail vein by means of a small incision with a scalpel blade and collected into EDTA-coated tubes. Complete blood counts were obtained with an Element HT5 hematology analyzer (Heska, USA).

Data reporting

Mice were randomly assigned to control and intervention groups. No statistical methods were used to predetermine sample size but group size was chosen based on variance of previous experiments. The investigators were blinded to genotype allocation during experiments and outcome assessment unless otherwise stated.

µCT analysis

To evaluate bone microarchitecture and osmium tetroxide (OsO_4) stains, a SkyScanner 1276 (Bruker, Belgium) was used. For both applications, a 0.25 mm Al filter was used with a voltage of 200 kV and a current of 55 mA. Samples were wrapped in PBS-soaked paper towels and scanned inside a plastic drinking straw sealed on both ends to avoid drying. Voxel size for both applications was set at 10×10×10 μm^3.

Bone microarchitecture was evaluated according to the ASBMR guidelines[95] using a custom CTan (Bruker, Belgium) script for automatic segmentation of trabecular bone in the distal femoral VOI, which was set 100 slices proximal to the distal growth plate and extended 200 slices towards the femoral diaphysis (slice thickness of 0.010 mm). The threshold used to binarize the calcified trabecular issue was 40 on a 0-255 scale. Reconstruction of the scans was performed using NRecon (Bruker, Belgium) and further analysis was performed using CTan (Bruker, Belgium) with the minimum for CS to image conversion set at 0 and maximum set at 0.14. For the analysis of cortical parameters, the midpoint of the femur was determined, and the VOI was defined as the bone 50 slices (slice thickness of 0.010 mm) distal and proximal of the slice corresponding to the midpoint of the bone. All other reconstruction parameters were kept the same as for the analysis of trabecular bone. The threshold used to binarize the calcified trabecular issue was 110 on a 0-255 scale. We provide a representative log file for bones analyzed with the trabecular and the cortical segmentation scripts for reference.

OsO_4 staining was performed on formalin-fixed, EDTA-decalcified tibias and caudal spines. For this, bones were kept in 10% formalin for 24 h at 4 °C. Following fixation, the bones were decalcified in PBS-0.5 M EDTA for 2 weeks, refreshing the decalcifying solution on day 7. OsO_4 staining was performed as previously described[49]. Reconstruction of the scans was performed as for calcified bone except for the minimum and maximum CS range, which was set to 0 and 0.30, respectively. OsO_4 was segmented using a threshold of 50 on a 0-255 scale. Images and quantification of BMAT were analyzed using Dragonfly software (ORS, Canada).

Flow cytometry

All antibodies used for this work as well as their dilutions are listed in the key resources table. All dilutions and cell suspensions were prepared in FACS buffer (2% FBS + 1 mM EDTA in PBS).

Histology

Spleens and thymi were fixed in 10% formalin for 24 h at 4 °C. EDTA-decalcified bones (as described previously for OsO_4 stain), spleens and thymi were cut longitudinally in 3-4 µm sections for staining. For immunohistochemistry (IHC), detection of rabbit anti-GFP as performed manually. After quenching with 3% H_2O_2 in PBS 1x for 10 min, a heat pretreatment using 0.1 M Tri-Na citrate pH 6 was applied at 60 °C in a water bath overnight. Primary antibodies were incubated overnight at 4 °C. After incubation of ImmPRESS HRP (Ready to use, Vector Laboratories), revelation was performed with DAB (3,3'-Diaminobenzidine, D5905, Sigma-Aldrich). Sections were counterstained with Harris hematoxylin and permanently mounted. All slides were imaged on an automated slide scanner (Olympus VS120-SL) at 20x or 40x.

Cell culture

Cell extraction

Culture of primary BMSCs was performed as reported in the literature[96]. 8- to 12-week-old male mice were used for these experiments. To isolate BMSCs from the BM, we collected femora and tibias, cut the epiphyses, and placed the bones in a 200 µL pipette tip with its end cut to fit in a 1.5

mL microcentrifuge tube. Bones were spun at 10.000 g for 10 sec to flush out the BM from the medullary cavity. The BM plug was then transferred to a 15 mL conical tube containing 10 mL of ascorbic-acid free αMEM (containing 10% FBS and 1% penicillin-streptomycin) and this suspension filtered through a 70 µm mesh filter prior to plating in a 100 mm cell culture dish (Corning, USA). Cells were replated 72 h later at a density of 62.500 cells/cm^2 in tissue-culture treated 12-well plates (i.e., 250.000 cells/well) and grown to confluency prior to differentiation, which usually occurred at one week post-replating. Culture medium was refreshed every other day until confluency[96].

For CFU-F assays, BM was obtained in a similar manner and plated at a density of 1 million cells per well of a tissue-culture treated 6-well plate (i.e., 100.000 cells/cm^2). CFU-F cultures were kept in αMEM containing 10% FBS and 1% penicillin-streptomycin and stained on day 7 post-plating with 0.1% toluidine blue in 10% formalin.

Media composition and differentiation cocktail

Differentiation into osteoblasts was started once confluency was reached. For osteoblastic differentiation, the base culture medium of ascorbic-acid free αMEM containing 10% FBS and 1% penicillin-streptomycin was supplemented with L-ascorbic acid (final concentration 8 mM) and β-glycerophosphate (final concentration 1 mM) and refreshed every other day until the endpoint of the assay. Dexamethasone was not included in the differentiation cocktail, as per the published protocol we followed[96].

Differentiation into adipocytes was started once confluency was reached. For adipocytic differentiation, base culture medium was high-glucose (4.5 g/L) DMEM supplemented with 10% FBS and 1% penicillin-streptomycin. Adipocytic induction medium containing dexamethasone (1 µM), isobutylmethylxanthine (IBMX, 0.5 mM), insulin (2 µM) and rosiglitazone (20 µM) was prepared. Cells were cultured in adipocytic differentiation medium for 4 days with refreshing on day 2. On day 4, culture medium was changed to maintenance medium, prepared by supplementing the base medium with only insulin (2 µM) and rosiglitazone (20 µM). Cells were kept in maintenance medium until the endpoint (day 7 post-differentiation) with no medium refreshing.

Differentiation stains

For alkaline phosphatase (ALP) stain of osteoblast cultures, one tablet of SigmaFast (Sigma-Aldrich) was dissolved in 10 mL distilled water. Osteoblasts were fixed in 10% formalin for 1 min, washed once with PBS-0.05% Tween 20 and incubated in the staining solution for 6 min. Cells were then washed with PBS-0.05% Tween 20 and imaged.

For alizarin red (AR) stain of calcium deposits in osteoblastic cultures after ALP staining, cells were washed once with distilled water and incubated for 45 min with AR stain (prepared fresh with 2 g of AR in 100 mL distilled water and pH adjusted to 4.2). Cells were then washed with distilled water 4 times and imaged.

For Oil Red O (ORO) staining of adipocyte cultures, we fixed the cells in 10% formalin for 1 h at room temperature. In the meantime, we filtered the ORO stock solution through filter paper as described in the literature[96]. Cells were stained with ORO for 15 min, washed 6 times with distilled water, imaged, and incubated for 10 min with 100% isopropanol to solubilize the stain. ORO was quantified using an iD3 plate reader (Agilent, USA) set to measure absorbance at 490 nm[96].

Digital holographic microscopy

Digital holographic imaging was performed in black wall 96-well imaging plates (Corning, 353962) using Transmission DHM® T1000 (Lyncée Tec, Switzerland).

Plates were pre-coated with Poly-ornithine (Sigma,100 mg/L) to prevent cell detachment. The cells were imaged live and without prior liquid manipulation using a 20x/0.4 NA microscope objective. The best-focus phase images were reconstructed automatically in MATLAB (MathWorks, USA) from the acquired holograms and the average quantitative phase signal or optical path difference (OPD) was automatically measured using a fixed threshold value.

Statistics

Differences in groups were assessed as stated in the legend for each figure. GraphPad Prism 9 was used for all statistical analyses. Before data analysis, outliers were checked, identified and excluded by using the Grubbs method (α value = 0.05) in GraphPad Prism 9. The data sheets provided with this work include the points flagged as outliers.

In Figure 5B and C, one animal from each genotype was excluded from analysis in "proximal tibia BMAT" and "total tibia BMAT" as the proximal epiphyses were avulsed upon dissection; these animals were kept for "distal BMAT" analyses as this part of the bone was intact.

The studies were either replicated and/or the results were confirmed by using different approaches (flow cytometry and IHC, for example) yielding similar results. All P values ≤ 0.05 were considered significant. When the exact value is not provided, *P ≤ 0.05, **P ≤ 0.01, ***P ≤ 0.001 and ****P ≤ 0.0001.

Data availability

Source data will be deposited in Zenodo upon acceptance, and available with all the Laboratory of Regenerative Hematopoiesis primary datasets also through *https://orcid.org/0000-0003-3434-0022*

Figure supplements

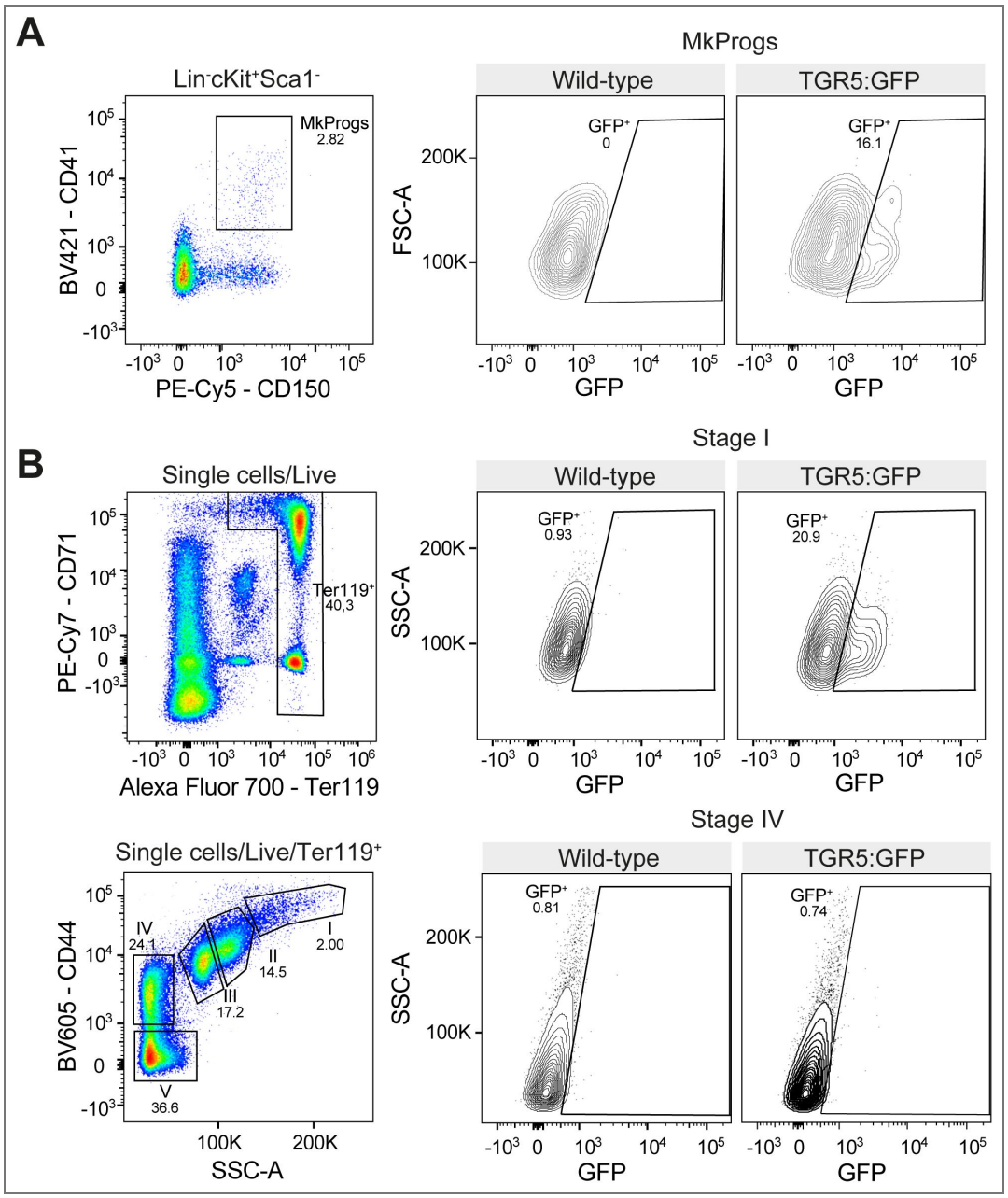

Figure 1-figure supplement 1. TGR5 is expressed in hematopoietic progenitors in the bone marrow. (**A**) Representative flow cytometry gating strategy used to identify megakaryocyte progenitors (MkProgs) in BM and their GFP positivity in TGR5:GFP mice. (**B**) Representative flow cytometry gating strategy used to identify cells in the different stages of erythropoiesis in BM and their GFP positivity in TGR5:GFP mice.

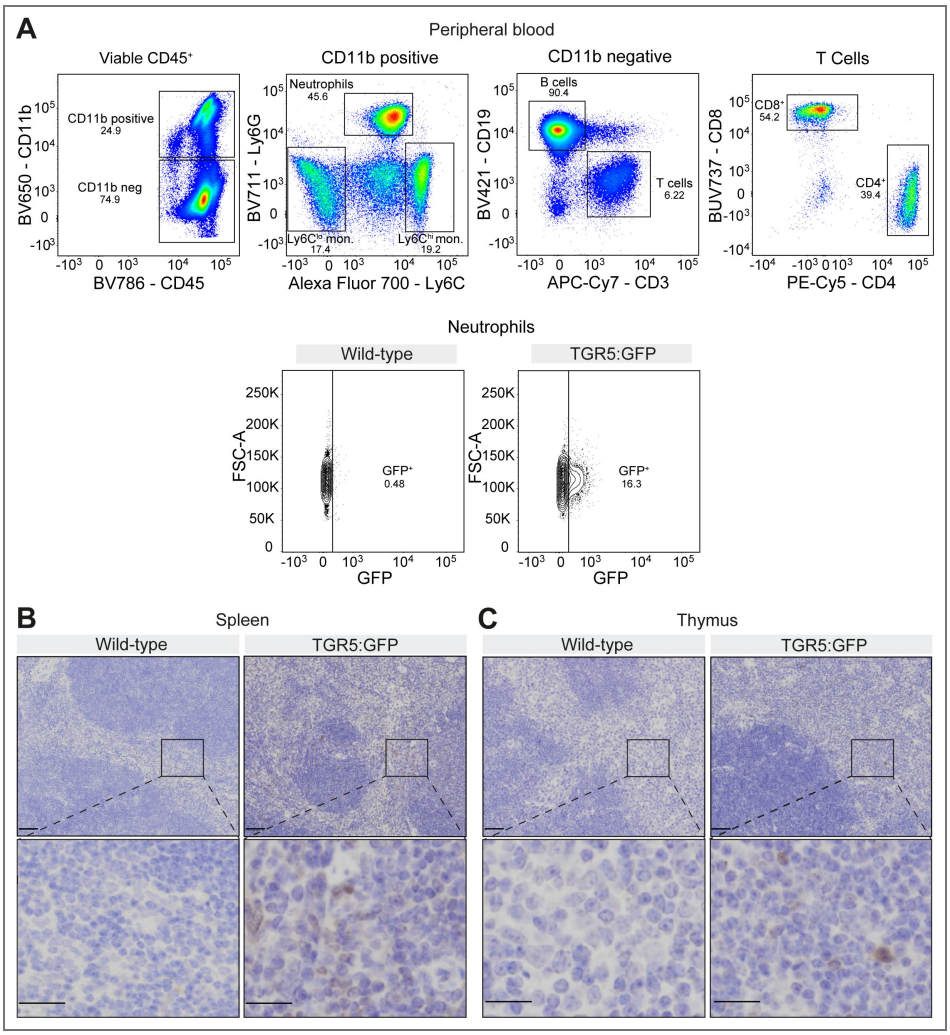

Figure 1-figure supplement 2. TGR5 is expressed in spleen, thymus and differentiated hematopoietic populations.

(**A**) Representative flow cytometry gating strategy used to identify differentiated populations in peripheral blood and GFP positivity in TGR5:GFP mice. (**B**, **C**) Immunodetection of GFP$^+$ cells by DAB IHC in spleen (**B**) and thymus (**C**) of 8- to 12-week-old male TGR5:GFP mice (n=2 for wild-type mice, n=3 for TGR5:GFP mice). Scale bar: 50 µm in low magnification images, 20 µm in the corresponding digitally zoomed images.

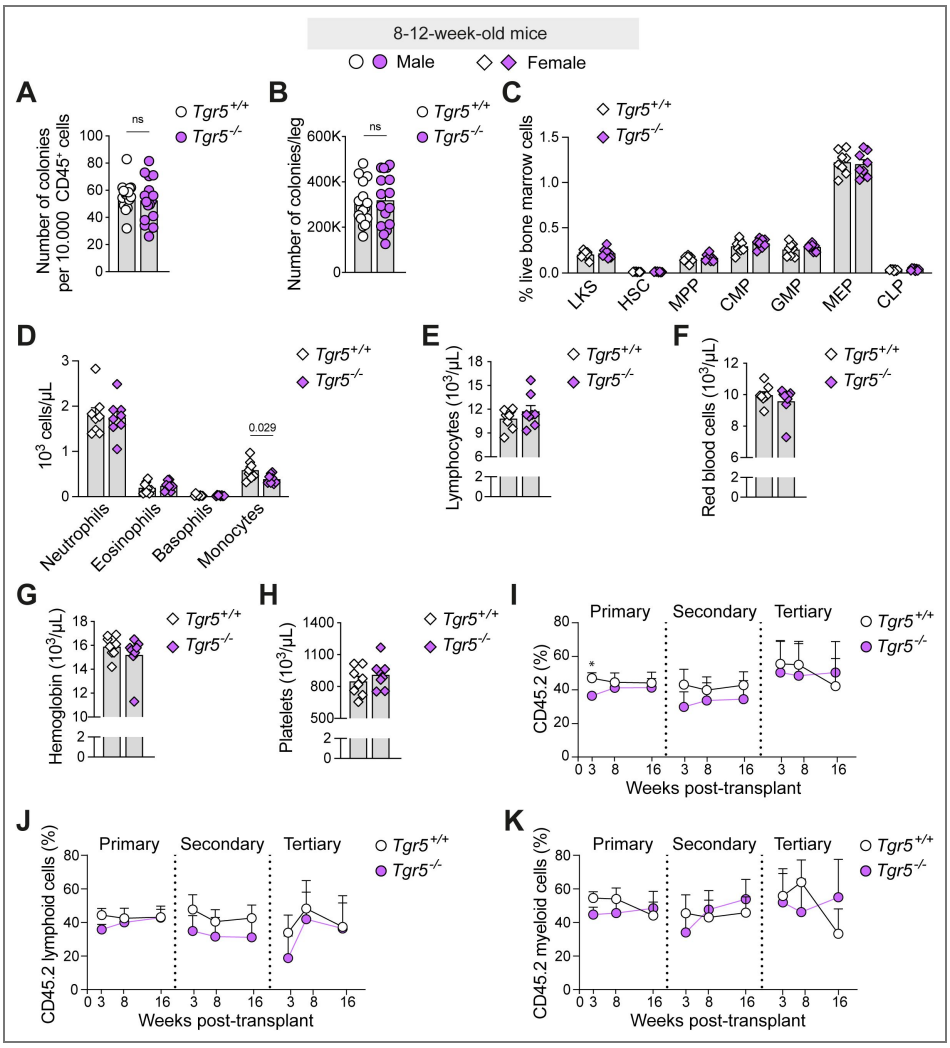

Figure 2-figure supplement 1. Loss of TGR5 does not impair steady-state hematopoiesis but compromises hematopoietic progenitor function in stress hematopoiesis.

(**A, B**) Number of colonies per 10.000 BM CD45$^+$ cells (**A**) and per leg (**B**) (n=16 for both *Tgr5*$^{+/+}$ and *Tgr5*$^{-/-}$ mice). (**C**) Frequency of hematopoietic stem and progenitor (HSPC) populations in the BM of 8-week-old *Tgr5*$^{+/+}$ and *Tgr5*$^{-/-}$ female mice expressed as percentage of cells over total live cells acquired (n=8 for both *Tgr5*$^{+/+}$ and *Tgr5*$^{-/-}$ mice). (**D-H**) Complete blood counts in peripheral blood of 8-week-old *Tgr5*$^{+/+}$ and *Tgr5*$^{-/-}$ female mice; myeloid cells (**D**), lymphocytes (**E**), red blood cells (**F**), hemoglobin (**G**), and platelets (**H**). (**I-K**) Flow cytometry analysis of peripheral blood chimerism expressed as the percentage of CD45.2 (**I**), CD45.2 lymphoid (**J**) and CD45.2 myeloid (**K**) cells of serial BM transplantation experiments (n=8, 8-12-week-old *Tgr5*$^{+/+}$ and *Tgr5*$^{-/-}$ male donors transplanted into 3 CD45.1 recipient mice each) at 3, 8 and 16 weeks post-transplant. Results represent the mean ± s.e.m., n represents biologically independent replicates. Unpaired, two-tailed Student's t-test was used for statistical analysis. *, p<0.05, ns indicates non-significance.

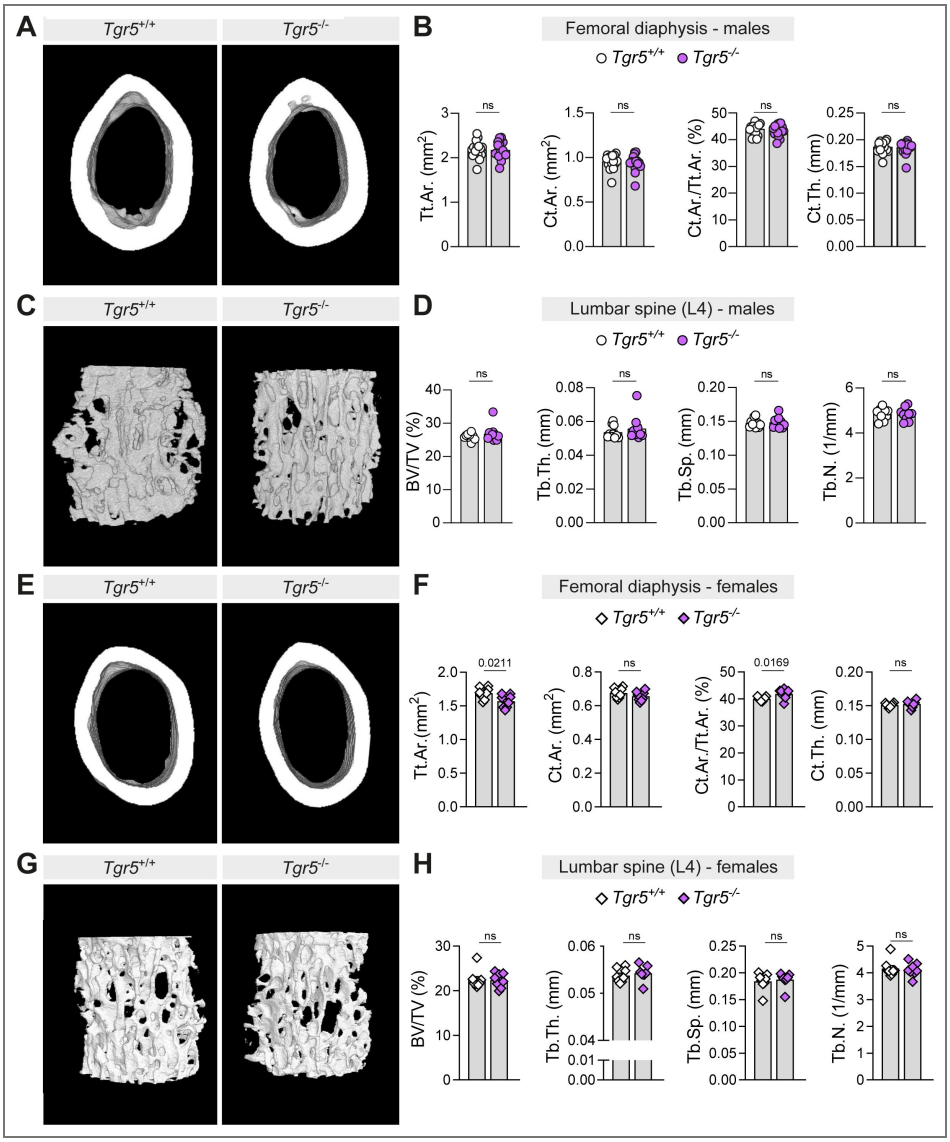

Figure 3-figure supplement 1. Loss of TGR5 did not alter the femoral cortical parameters or the spine microarchitecture.

(**A**) Representative native µCT-derived 3D reconstructions of the cortical bone in the mid-femoral diaphysis of 8- to 12-week-old *Tgr5*$^{+/+}$ and *Tgr5*$^{-/-}$ male mice. (**B**) µCT-derived bone morphometry measurements of the cortical bone in the mid-femoral diaphysis of 8- to 12-week-old *Tgr5*$^{+/+}$ and *Tgr5*$^{-/-}$ male mice (n=17 for both *Tgr5*$^{+/+}$ and *Tgr5*$^{-/-}$ mice); shown are the total cross-sectional area inside the periosteal envelope (Tt.Ar.), cortical bone area (Ct.Ar.), cortical area fraction (Ct.Ar./Tt.Ar.) and average cortical thickness (Ct.Th.). **(C)** Representative native µCT-derived 3D reconstructions of the trabecular structures in the fourth lumbar vertebrae (L4) of 8- to 12-week-old *Tgr5*$^{+/+}$ and *Tgr5*$^{-/-}$ male mice. **(D)** µCT-derived bone morphometry measurements of the trabecular structures in L4 of 8- to 12-week-old *Tgr5*$^{+/+}$ and *Tgr5*$^{-/-}$ male mice (n=10 for both *Tgr5*$^{+/+}$ and *Tgr5*$^{-/-}$ mice); shown are bone volume/total volume (BV/TV), trabecular thickness (Tb.Th.), trabecular separation (Tb.Sp.) and trabecular number (Tb.N.). (**E**) Representative native µCT-derived 3D reconstructions of the cortical bone in the mid-femoral diaphysis of 8-week-old *Tgr5*$^{+/+}$ and *Tgr5*$^{-/-}$ female mice. (**F**) µCT-derived bone morphometry measurements of the cortical bone in the mid-femoral diaphysis of 8-week-old *Tgr5*$^{+/+}$ and *Tgr5*$^{-/-}$ female mice (n=8 for both *Tgr5*$^{+/+}$ and *Tgr5*$^{-/-}$ mice); parameters shown analogously to **B**. (**G**) Representative native µCT-derived 3D reconstructions of the trabecular structures in the fourth lumbar vertebrae (L4) of 8-week-old *Tgr5*$^{+/+}$ and *Tgr5*$^{-/-}$ female mice. (**H**) µCT-derived bone morphometry measurements of the trabecular structures in L4 of 8-week-old *Tgr5*$^{+/+}$ and *Tgr5*$^{-/-}$ female mice (n=8 for both *Tgr5*$^{+/+}$ and *Tgr5*$^{-/-}$ mice); parameters shown analogously to **D**. Results represent the mean ± s.e.m., n represents biologically independent replicates. Unpaired, two-tailed Student's t-test **(B, D, F, H)** was used for statistical analysis. P values (exact value) are indicated, ns indicates no statistical significance.

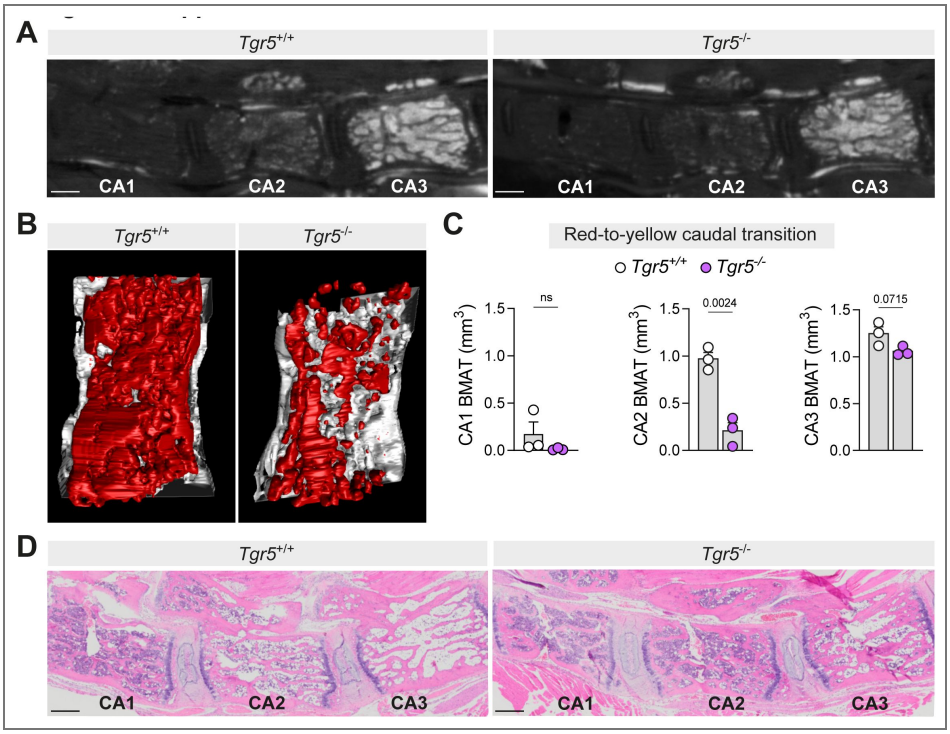

Figure 3-figure supplement 2. Loss of TGR5 alters the BM microenvironment in the caudal spine.

(**A**) Representative images obtained from contrast-enhanced µCT scanning of decalcified OsO_4-stained spines depicting lipid content in the red-to-yellow marrow transition in the caudal spine (CA) of 14-week-old male *Tgr5*$^{+/+}$ and *Tgr5*$^{-/-}$ mice. (**B**) Sagittal view of a representative contrast-enhanced µCT-derived 3D reconstruction of OsO_4-stained BMAT in the second caudal vertebrae (CA2) of 14-week-old *Tgr5*$^{+/+}$ and *Tgr5*$^{-/-}$ male mice. (**C**) Quantification of the OsO_4-stained BMAT for the first to third caudal vertebra (CA1-CA3) in the caudal red-to-yellow transition in 14-week-old *Tgr5*$^{+/+}$ and *Tgr5*$^{-/-}$ male mice (n=3 for both *Tgr5*$^{+/+}$ and *Tgr5*$^{-/-}$ mice). (**D**) Representative hematoxylin & eosin (H&E) histological sections of CA1-CA3 from a cohort independent from the animals shown in **A-C** (n=4 for both *Tgr5*$^{+/+}$ and *Tgr5*$^{-/-}$ mice, 11- to 13-week-old). Scale bar in **A** and **D** = 500 µm. Results represent the mean ± s.e.m., n represents biologically independent replicates. Unpaired, two-tailed Student's t-test **(C)** was used for statistical analysis. P values (exact value) are indicated, ns indicates no statistical significance.

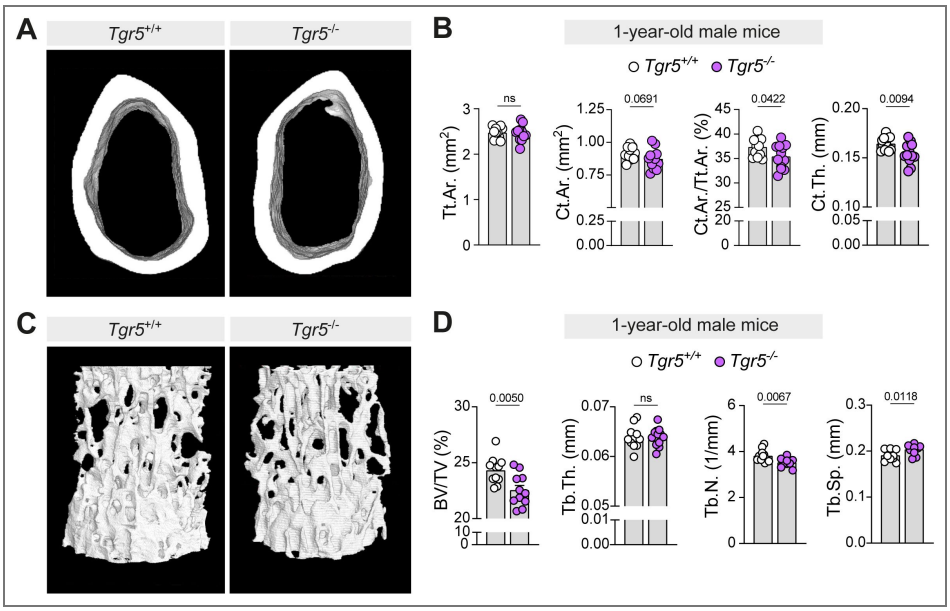

Figure 4-figure supplement 1. Loss of TGR5 slightly decreases vertebral and femoral cortical mineralized tissue in 1-year-old male mice.

(**A**) Representative native µCT-derived 3D reconstructions of the cortical bone in the mid-femoral diaphysis of 1-year-old *Tgr5*$^{+/+}$ and *Tgr5*$^{-/-}$ male mice. (**B**) µCT-derived bone morphometry measurements of the cortical bone in the mid-femoral diaphysis of 1-year-old *Tgr5*$^{+/+}$ and *Tgr5*$^{-/-}$ male mice (n=12 for both *Tgr5*$^{+/+}$ and *Tgr5*$^{-/-}$ mice); shown are the total cross-sectional area inside the periosteal envelope (Tt.Ar.), cortical bone area (Ct.Ar.), cortical area fraction (Ct.Ar./Tt.Ar.) and average cortical thickness (Ct.Th.). (**C**) Representative native µCT-derived 3D reconstructions of the trabecular structures in the fourth lumbar vertebrae (L4) of 1-year-old *Tgr5*$^{+/+}$ and *Tgr5*$^{-/-}$ male mice. (**D**) µCT-derived bone morphometry measurements of the trabecular structures in L4 of 1-year-old *Tgr5*$^{+/+}$ and *Tgr5*$^{-/-}$ male mice (n=12 for both *Tgr5*$^{+/+}$ and *Tgr5*$^{-/-}$ mice); shown are bone volume/total volume (BV/TV), trabecular thickness (Tb.Th.), trabecular number (Tb.N.) and trabecular separation (Tb.Sp.). Results represent the mean ± s.e.m., n represents biologically independent replicates. Unpaired, two-tailed Student's t-test (**B**, **D**) was used for statistical analysis. P values (exact value) are indicated, ns indicates no statistical significance.

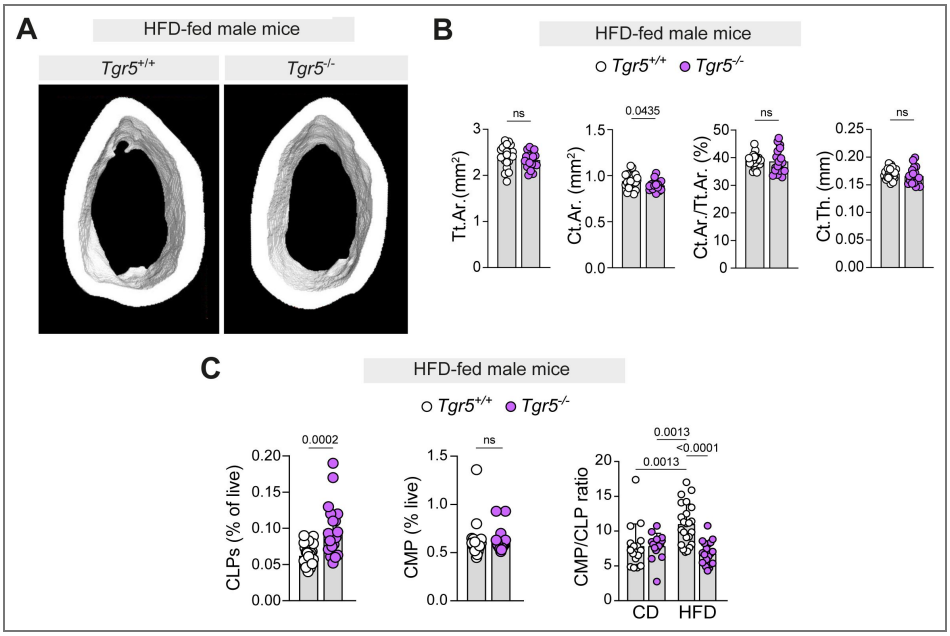

Figure 5-figure supplement 1. Loss of TGR5 does not affect femoral cortical parameters and blunts BM HSPC myeloid bias in HFD-fed male mice.

(**A**) Representative native µCT-derived 3D reconstructions of the cortical bone in the mid-femoral diaphysis of HFD-fed (12 weeks) *Tgr5*$^{+/+}$ and *Tgr5*$^{-/-}$ male mice. (**B**) µCT-derived bone morphometry measurements of the cortical bone in the mid-femoral diaphysis of HFD-fed (12 weeks) *Tgr5*$^{+/+}$ and *Tgr5*$^{-/-}$ male mice (n=24 for *Tgr5*$^{+/+}$ and n=18 for *Tgr5*$^{-/-}$ mice); shown are the total cross-sectional area inside the periosteal envelope (Tt.Ar.), cortical bone area (Ct.Ar.), cortical area fraction (Ct.Ar./Tt.Ar.) and average cortical thickness (Ct.Th.). (**C**) Frequency of common lymphoid progenitors (CLP), common myeloid progenitors (CMP) and ratio of CMP-to-CLP cells in the BM of CD-fed (calculated from the data presented in Figure 2A, same data as the "8- to 12-week-old" group in Figure 4F) and HFD-fed *Tgr5*$^{+/+}$ and *Tgr5*$^{-/-}$ mice (n=24 for *Tgr5*$^{+/+}$ and n=20 for *Tgr5*$^{-/-}$ mice). Results represent the mean ± s.e.m., n represents biologically independent replicates. Unpaired, two-tailed Student's t-test was used for statistical analysis except for last panel in **C**, where a 2-way ANOVA test with Holm-Sidak's multiple comparison correction was used. P values (exact value) are indicated, ns indicates no statistical significance.

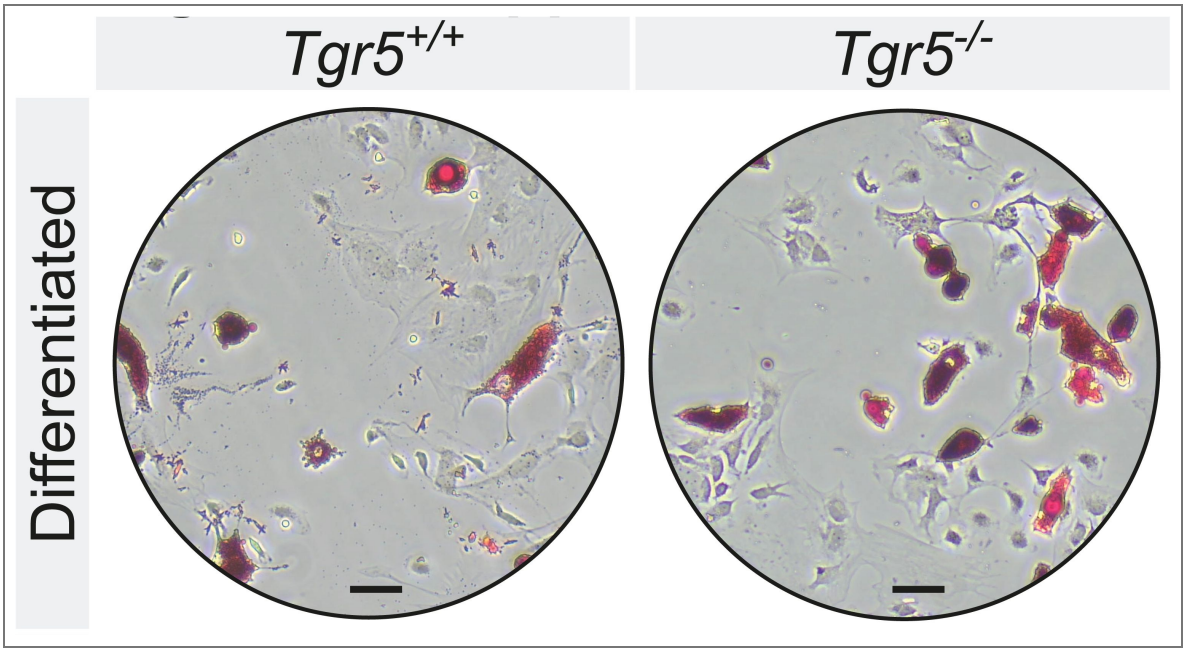

Figure 6-figure supplement 1. Loss of TGR5 increases in vitro BMSC differentiation into adipocytes.

(A) Representative images of Oil red O (ORO)-stained BMSCs after 7 days of adipocytic differentiation (n=3 for both *Tgr5*$^{+/+}$ and *Tgr5*$^{-/-}$ mice). Scale bar: 50 µm.

Key Resources Table.

Reagent type. Duplicate rows as needed. Order is flexible, but row titles must be preserved. **Species** (mandatory if applicable). Append in parentheses. First mention, use full genus. **Sex** (if applicable). Add within parentheses after species.	**Designation.** Symbol/name used in publication. Separate multiple entries with semi-colon, space. (If semi-colon within designation, delimit with double quotes.)	**Source (public).** Stock center, company, data repository. **Reference.** Include PMID or DOI; use "this paper" if new. **If neither** applies enter "other" and explain in Additional Information.	**Identifiers.** Format as *ID_source:identifier*. Separate multiple entries with semi-colon, space. Include catalog numbers, stock numbers, database IDs or accession numbers, RRIDs.	**Additional information.** Mandatory if column C entry is "this paper" or "other". Description of new reagent; laboratory from which reagent obtained; other pertinent information. For antibodies, indicate dilution and conditions used.
Reagent type (species) or resource	**Designation**	**Source or reference**	**Identifiers**	**Additional information**
gene ()		NA		
strain, strain background (*Mus musculus*)	TGR5:GFP			
strain, strain background (*Mus musculus*)	TGR5 knock-out mouse model (*Tgr5*$^{-/-}$)			
strain, strain background (*Mus musculus*)	C57BL/6J (CD45.2)			
strain, strain background (*Mus musculus*)	C57BL/6J Ly5.1 (CD45.1)			
strain, strain background (*Mus musculus*)	congenic mice (CD45.1.2)			
genetic reagent ()				
cell line ()				
transfected construct ()				
biological sample ()				
antibody	Biotin lineage cocktail	BD Biosciences	51-9000724	
antibody	Streptavidin - Texas Red	Invitrogen	S872	
antibody	cKit - PE/Cy7	Biolegend	105814	
antibody	Sca1 - BV711	BD Biosciences	563992	
antibody	CD150 - PE/Cy5	Biolegend	115912	
antibody	CD48 - Pacific Blue	Biolegend	103418	
antibody	CD34 - eFluor 660	Invitrogen	50-0314-82	
antibody	CD127 - PE	Invitrogen	12-1271-83	
antibody	CD16/32 - Alexa Fluor700	Invitrogen	56-0161-82	
antibody	Sca1 - APC	Biolegend	105112	
antibody	PDGFRa - PE	Biolegend	135905	
antibody	CD45 - Alexa Fluor700	Biolegend	103128	
antibody	Ter119 - Alexa Fluor 700	Biolegend	116220	
antibody	CD24 APC eFluor780	Invitrogen	47-0242-82	
antibody	CD31 - PE/Cy7	Biolegend	102418	
antibody	CD45 - BV785	Biolegend	103149	
antibody	CD11b - BV650	Biolegend	101239	
antibody	Ly6G - BV711	Biolegend	127643	
antibody	Ly6C - Alexa Fluor 700	Biolegend	128024	
antibody	CD4 - PE/Cy5	Biolegend	100410	
antibody	CD19 - BV421	BD Biosciences	562440	
antibody	CD8 - BUV737	BD Biosciences	612759	
antibody	CD3 - APC/Cy7	Biolegend	100222	
antibody	GFP	Abcam	ab6673	
antibody				
recombinant DNA reagent				
sequence-based reagent				
peptide, recombinant protein				
commercial assay or kit	SigmaFast	Sigma-Aldrich		
commercial assay or kit				
chemical compound, drug	Dafalgan			
chemical compound, drug	Osmium tetroxide (OsO_4)			
chemical compound, drug	Formalin			10%
chemical compound, drug	EDTA			
chemical compound, drug				
chemical compound, drug				
chemical compound, drug				
software, algorithm	Prism	GraphPad	Prism 9	
software, algorithm	Custom CTan script	Bruker, Belgium		
software, algorithm	NRecon	Bruker, Belgium		
software, algorithm	Dragonfly software	ORS, Canada		
software, algorithm	MATLAB	MathWorks, USA		
other	Chow Diet	SAFE	SAFE 150	
other	High Fat Diet	Research Diets	D12492	
other	RS-2000 X-ray irradiator	RAD SOURCE		
other	EDTA-coated tubes			
other	Element HT5 hematology analyzer	Heska, USA		
other	SkyScanner 1276	Bruker, Belgium		
other	FACS buffer			2% serum + 1 mM EDTA in PBS
other	PBS			
other	3% H_2O_2			
other	0.1 M Tri-Na citrate			
other	ImmPRESS HRP	Vector Laboratories		
other	3,3'-Diaminobenzidine	Sigma-Aldrich	D5905	
other	Harris hematoxylin			
other	Slide scanner	Olympus VS120-SL		
other	Ascorbic-acid free aMEM			
other	FBS			
other	Penicillin-streptomycin			
other	Toluidine blue			
other	L-ascorbic acid			
other	β-glycerophosphate			
other	high-glucose (4.5 g/L) DMEM			
other	dexamethasone			
other	isobutylmethylxanthine			
other	insulin			
other	rosiglitazone			
other	Tween 20			
other	alizarin red			
other	Oil Red O (ORO)			
other	iD3 plate reader	Agilent, USA		
other	black wall 96-well imaging plates	Corning	353962	
other	Transmission DHM® T1000	Lyncée Tec, Switzerland		
other	Poly-ornithine	Sigma-Aldrich		
other				

Antibodies flow cytometry (anti-mouse)	Commercial source	Cat.no
Biotin lineage cocktail	BD Biosciences	51-9000724
Streptavidin - Texas Red	Invitrogen	S872
cKit - PE/Cy7	Biolegend	105814
Sca1 - BV711	BD Biosciences	563992
CD150 - PE/Cy5	Biolegend	115912
CD48 - Pacific Blue	Biolegend	103418
CD34 - eFluor 660	Invitrogen	50-0314-82
CD127 - PE	Invitrogen	12-1271-83
CD16/32 - Alexa Fluor700	Invitrogen	56-0161-82
Sca1 - APC	Biolegend	105112
PDGFRa - PE	Biolegend	135905
CD45 - Alexa Fluor700	Biolegend	103128
Ter119 - Alexa Fluor 700	Biolegend	116220
CD24 APC eFluor780	Invitrogen	47-0242-82
CD31 - PE/Cy7	Biolegend	102418
CD45 - BV785	Biolegend	103149
CD11b - BV650	Biolegend	101239
Ly6G - BV711	Biolegend	127643
Ly6C - Alexa Fluor 700	Biolegend	128024
CD4 - PE/Cy5	Biolegend	100410
CD19 - BV421	BD Biosciences	562440
CD8 - BUV737	BD Biosciences	612759
CD3 - APC/Cy7	Biolegend	100222

Acknowledgements

We wish to thank the Histology Core Facility, Center for Phenogenomics, Bioscreening Facilities, Electron Microscopy facilities and BioImaging and Optics Platform at EPFL as well as the In Vivo and Cellular Imaging Facilities at AGORA (UNIL/EPFL) and the Flow Cytometry Facility at AGORA (UNIL/EPFL) for their continuous support and guidance for this project, as well as Dr. Frédéric Schütz (UNIL) for guidance on statistical analysis. This work was funded by the Ecole Polytechnique Fédérale de Lausanne (EPFL), the University of Lausanne (UNIL), the Swiss National Science Foundation (SNSF N° 310030_189178, Sinergia CRSII5_180317/1 to K.S. and SNSF N° PP00P3_144857, 183725 and 320030-231787 to O.N.), and La Caixa Foundation (to K.S.). Alessia Perino was supported by a fellowship from AXA Research Fund. Frédérica Schyrr was funded by SNSF MD-PhD grant 183986.

Additional information

Author contribution

AAC, AP and FS: Data curation, Formal analysis, Investigation, Methodology, Writing – original draft, writing – review and editing. SFL, VD, AJ, UK, MCG, AM, CB, DPP: Methodology. KS and ON Conceptualization, Resources, Supervision, Funding acquisition, Validation, Investigation, Writing – original draft, Project administration, Writing – review and editing.

Funding

Funder	Grant reference number	Author
Schweizerischer Nationalfonds zur Förderung der Wissenschaftlichen Forschung (SNF)	310030_189178	Kristina Schoonjans
Schweizerischer Nationalfonds zur Förderung der Wissenschaftlichen Forschung (SNF)	CRSII5_180317/1	Kristina Schoonjans
Schweizerischer Nationalfonds zur Förderung der Wissenschaftlichen Forschung (SNF)	PP00P3_183725	Olaia Naveiras
Schweizerischer Nationalfonds zur Förderung der Wissenschaftlichen Forschung (SNF)	320030-231787	Olaia Naveiras
'la Caixa' Foundation ('la Caixa')		Kristina Schoonjans
AXA Research Fund (FONDS AXA POUR LA RECHERCHE)		Alessia Perino
Schweizerischer Nationalfonds zur Förderung der Wissenschaftlichen Forschung (SNF)		Frédérica Schyrr

Author ORCID iDs

Dominique P Pioletti: https://orcid.org/0000-0001-5535-5296
Kristina Schoonjans: https://orcid.org/0000-0003-1247-4265
Olaia Naveiras: https://orcid.org/0000-0003-3434-0022

References

1. **Pinho S,** Frenette PS (2019) Haematopoietic stem cell activity and interactions with the niche. *Nat Rev Mol Cell Biol* **20**:303-320 https://doi.org/10.1038/s41580-019-0103-9 | PubMed
2. **Bolamperti S,** Villa I, Rubinacci A (2022) Bone remodeling: an operational process ensuring survival and bone mechanical competence. *Bone Res* **10**:48 https://doi.org/10.1038/s41413-022-00219-8 | PubMed

3. **Karsenty G,** Khosla S (2022) The crosstalk between bone remodeling and energy metabolism: A translational perspective. *Cell Metab* **34**:805-817 https://doi.org/10.1016/j.cmet.2022.04.010 | PubMed
4. **Karsenty G,** Oury F (2010) The central regulation of bone mass, the first link between bone remodeling and energy metabolism. *J Clin Endocrinol Metab* **95**:4795-4801 https://doi.org/10.1210/jc.2010-1030 | PubMed
5. **Baccin C,** et al. (2020) Combined single-cell and spatial transcriptomics reveal the molecular, cellular and spatial bone marrow niche organization. *Nat Cell Biol* **22**:38-48 https://doi.org/10.1038/s41556-019-0439-6 | PubMed
6. **Naveiras O,** et al. (2009) Bone-marrow adipocytes as negative regulators of the haematopoietic microenvironment. *Nature* **460**:259-263 https://doi.org/10.1038/nature08099 | PubMed
7. **Zhou BO,** et al. (2017) Bone marrow adipocytes promote the regeneration of stem cells and haematopoiesis by secreting SCF. *Nat Cell Biol* **19**:891-903 https://doi.org/10.1038/ncb3570 | PubMed
8. **Yu W,** et al. (2021) Bone marrow adipogenic lineage precursors promote osteoclastogenesis in bone remodeling and pathologic bone loss. *J Clin Invest* **131**:e140214 https://doi.org/10.1172/jci140214 | PubMed
9. **Zhong L,** et al. (2020) Single cell transcriptomics identifies a unique adipose lineage cell population that regulates bone marrow environment. *eLife* **9**:e54695 https://doi.org/10.7554/eLife.54695 | PubMed
10. **Zhong L,** et al. (2023) Csf1 from marrow adipogenic precursors is required for osteoclast formation and hematopoiesis in bone. *eLife* **12**:e82112 https://doi.org/10.7554/eLife.82112 | PubMed
11. **Wilson A,** Trumpp A (2006) Bone-marrow haematopoietic-stem-cell niches. *Nat Rev Immunol* **6**:93-106 https://doi.org/10.1038/nri1779 | PubMed
12. **Gomariz A,** et al. (2018) Quantitative spatial analysis of haematopoiesis-regulating stromal cells in the bone marrow microenvironment by 3D microscopy. *Nat Commun* **9**:2532 https://doi.org/10.1038/s41467-018-04770-z | PubMed
13. **Morrison SJ,** Scadden DT (2014) The bone marrow niche for haematopoietic stem cells. *Nature* **505**:327-334 https://doi.org/10.1038/nature12984 | PubMed
14. **Zhu R.-J,** Wu M.-Q, Li Z.-J, Zhang Y, Liu K.-Y (2013) Hematopoietic recovery following chemotherapy is improved by BADGE-induced inhibition of adipogenesis. *Int J Hematol* **97**:58-72 https://doi.org/10.1007/s12185-012-1233-4 | PubMed
15. **Ambrosi TH,** et al. (2017) Adipocyte Accumulation in the Bone Marrow during Obesity and Aging Impairs Stem Cell-Based Hematopoietic and Bone Regeneration. *Cell Stem Cell* **20**:771-784.e6 https://doi.org/10.1016/j.stem.2017.02.009 | PubMed
16. **Wilson A,** et al. (2018) Lack of Adipocytes Alters Hematopoiesis in Lipodystrophic Mice. *Front Immunol* **9**:2573 https://doi.org/10.3389/fimmu.2018.02573 | PubMed
17. **Sato K,** et al. (2016) PPAR antagonist attenuates mouse immune-mediated bone marrow failure by inhibition of T cell function. *Haematologica* **101**:57-67 https://doi.org/10.3324/haematol.2014.121632 | PubMed
18. **Zhong L,** et al. (2022) Transient expansion and myofibroblast conversion of adipogenic lineage precursors mediate bone marrow repair after radiation. *JCI Insight* **7**:e150323 https://doi.org/10.1172/jci.insight.150323 | PubMed
19. **Hirakawa H,** Gao L, Tavakol DN, Vunjak-Novakovic G, Ding L (2023) Cellular plasticity of the bone marrow niche promotes hematopoietic stem cell regeneration. *Nat Genet* **55**:1941-1952 https://doi.org/10.1038/s41588-023-01528-2 | PubMed
20. **Cawthorn WP,** et al. (2016) Expansion of Bone Marrow Adipose Tissue During Caloric Restriction Is Associated With Increased Circulating Glucocorticoids and Not With Hypoleptinemia. *Endocrinology* **157**:508-521 https://doi.org/10.1210/en.2015-1477 | PubMed

21. **Tavassoli M** (1974) Differential response of bone marrow and extramedullary adipose cells to starvation. *Experientia* **30**:424-425 https://doi.org/10.1007/bf01921701 | PubMed

22. **Ackert-Bicknell CL,** et al. (2009) Strain-Specific Effects of Rosiglitazone on Bone Mass, Body Composition, and Serum Insulin-Like Growth Factor-I. *Endocrinology* **150**:1330-1340 https://doi.org/10.1210/en.2008-0936 | PubMed

23. **Austin MJ,** Kalampalika F, Cawthorn WP, Patel B (2023) Turning the spotlight on bone marrow adipocytes in haematological malignancy and non-malignant conditions. *Br J Haematol* **201**:605-619 https://doi.org/10.1111/bjh.18748 | PubMed

24. **Tratwal J,** et al. (2020) Reporting Guidelines, Review of Methodological Standards, and Challenges Toward Harmonization in Bone Marrow Adiposity Research. Report of the Methodologies Working Group of the International Bone Marrow Adiposity Society. *Front Endocrinol* **11**:65 https://doi.org/10.3389/fendo.2020.00065 | PubMed

25. **Zhang D,** et al. (2022) The microbiota regulates hematopoietic stem cell fate decisions by controlling iron availability in bone marrow. *Cell Stem Cell* **29**:232-247.e7 https://doi.org/10.1016/j.stem.2021.12.009 | PubMed

26. **Sjögren K,** et al. (2012) The gut microbiota regulates bone mass in mice. *J Bone Miner Res* **27**:1357-1367 https://doi.org/10.1002/jbmr.1588 | PubMed

27. **Quach D,** Collins F, Parameswaran N, McCabe L, Britton RA (2018) Microbiota Reconstitution Does Not Cause Bone Loss in Germ-Free Mice. *mSphere* **3**:e00545-17 https://doi.org/10.1128/mspheredirect.00545-17 | PubMed

28. **Luo Y,** et al. (2015) Microbiota from Obese Mice Regulate Hematopoietic Stem Cell Differentiation by Altering the Bone Niche. *Cell Metab* **22**:886-894 https://doi.org/10.1016/j.cmet.2015.08.020 | PubMed

29. **Collins SL,** Stine JG, Bisanz JE, Okafor CD, Patterson AD (2023) Bile acids and the gut microbiota: metabolic interactions and impacts on disease. *Nat Rev Microbiol* **21**:236-247 https://doi.org/10.1038/s41579-022-00805-x | PubMed

30. **Kawamata Y,** et al. (2003) A G Protein-coupled Receptor Responsive to Bile Acids. *J Biol Chem* **278**:9435-9440 https://doi.org/10.1074/jbc.m209706200 | PubMed

31. **Perino A,** Demagny H, Velazquez-Villegas L, Schoonjans K (2021) Molecular physiology of bile acid signaling in health, disease, and aging. *Physiol Rev* **101**:683-731 https://doi.org/10.1152/physrev.00049.2019 | PubMed

32. **Perino A,** Schoonjans K (2022) Metabolic Messengers: bile acids. *Nat Metab* **4**:416-423 https://doi.org/10.1038/s42255-022-00559-z | PubMed

33. **Carino A,** et al. (2017) Gpbar1 agonism promotes a Pgc-1α-dependent browning of white adipose tissue and energy expenditure and reverses diet-induced steatohepatitis in mice. *Sci Rep* **7**:13689 https://doi.org/10.1038/s41598-017-13102-y | PubMed

34. **Velazquez-Villegas LA,** et al. (2018) TGR5 signalling promotes mitochondrial fission and beige remodelling of white adipose tissue. *Nat Commun* **9**:245 https://doi.org/10.1038/s41467-017-02068-0 | PubMed

35. **Perino A,** et al. (2014) TGR5 reduces macrophage migration through mTOR-induced C/EBPβ differential translation. *J Clin Invest* **124**:5424-5436 https://doi.org/10.1172/jci76289 | PubMed

36. **Eggink HM,** et al. (2018) Chronic infusion of taurolithocholate into the brain increases fat oxidation in mice. *J Endocrinol* **236**:85-97 https://doi.org/10.1530/joe-17-0503 | PubMed

37. **Broeders EPM,** et al. (2015) The Bile Acid Chenodeoxycholic Acid Increases Human Brown Adipose Tissue Activity. *Cell Metab* **22**:418-426 https://doi.org/10.1016/j.cmet.2015.07.002 | PubMed

38. **Watanabe M,** et al. (2006) Bile acids induce energy expenditure by promoting intracellular thyroid hormone activation. *Nature* **439**:484-489 https://doi.org/10.1038/nature04330 | PubMed

39. **Persaud AK,** et al. (2021) Facilitative lysosomal transport of bile acids alleviates ER stress in mouse hematopoietic precursors. *Nat Commun* **12**:1248 https://doi.org/10.1038/s41467-021-21451-6 | PubMed

40. **Sigurdsson V,** et al. (2016) Bile Acids Protect Expanding Hematopoietic Stem Cells from Unfolded Protein Stress in Fetal Liver. *Cell Stem Cell* **18**:522-532 https://doi.org/10.1016/j.stem.2016.01.002 | PubMed

41. **Sigurdsson V,** et al. (2020) Induction of blood-circulating bile acids supports recovery from myelosuppressive chemotherapy. *Blood Adv* **4**:1833-1843 https://doi.org/10.1182/bloodadvances.2019000133 | PubMed

42. **Thompson B,** et al. (2023) Secondary bile acids function through the vitamin D receptor in myeloid progenitors to promote myelopoiesis. *Blood Adv* bloodadvances.2022009618 https://doi.org/10.1182/bloodadvances.2022009618 | PubMed

43. **Perino A,** et al. (2021) Central anorexigenic actions of bile acids are mediated by TGR5. *Nat Metab* **3**:595-603 https://doi.org/10.1038/s42255-021-00398-4 | PubMed

44. **Chen K,** et al. (2009) Resolving the distinct stages in erythroid differentiation based on dynamic changes in membrane protein expression during erythropoiesis. *Proc Natl Acad Sci* **106**:17413-17418 https://doi.org/10.1073/pnas.0909296106 | PubMed

45. **Reusswig F,** et al. (2024) The bile acid receptor TGR5 inhibits platelet activation and thrombus formation. *Platelets* **35**:2322733 https://doi.org/10.1080/09537104.2024.2322733 | PubMed

46. **Li Z,** et al. (2018) Dual Targeting of Bile Acid Receptor-1 (TGR5) and Farnesoid X Receptor (FXR) Prevents Estrogen-Dependent Bone Loss in Mice. *J Bone Miner Res* jbmr.3652 https://doi.org/10.1002/jbmr.3652 | PubMed

47. **Nagano K,** et al. (2022) R-spondin 3 deletion induces Erk phosphorylation to enhance Wnt signaling and promote bone formation in the appendicular skeleton. *eLife* **11**:e84171 https://doi.org/10.7554/eLife.84171 | PubMed

48. **Berendsen AD,** Olsen BR (2015) Bone development. *Bone* **80**:14-18 https://doi.org/10.1016/j.bone.2015.04.035 | PubMed

49. **Scheller EL,** et al. (2014) Use of Osmium Tetroxide Staining with Microcomputerized Tomography to Visualize and Quantify Bone Marrow Adipose Tissue In Vivo. *Methods in Enzymology* **537**:123-139 https://doi.org/10.1016/b978-0-12-411619-1.00007-0 | PubMed

50. **Scheller EL,** et al. (2015) Region-specific variation in the properties of skeletal adipocytes reveals regulated and constitutive marrow adipose tissues. *Nat Commun* **6**:7808 https://doi.org/10.1038/ncomms8808 | PubMed

51. **Lovdel A,** et al. (2024) Deletion of Hsd11b1 suppresses caloric restriction-induced bone marrow adiposity in male but not female mice. *J Endocrinol* **262**:e240072 https://doi.org/10.1530/joe-24-0072 | PubMed

52. **Tratwal J,** et al. (2020) MarrowQuant Across Aging and Aplasia: A Digital Pathology Workflow for Quantification of Bone Marrow Compartments in Histological Sections. *Front Endocrinol* **11**:480 https://doi.org/10.3389/fendo.2020.00480 | PubMed

53. **Zhang Z,** et al. (2023) O-GlcNAc glycosylation orchestrates fate decision and niche function of bone marrow stromal progenitors. *eLife* **12**:e85464 https://doi.org/10.7554/eLife.85464 | PubMed

54. **Boroumand P,** et al. (2022) Bone marrow adipocytes drive the development of tissue invasive Ly6Chigh monocytes during obesity. *eLife* **11**:e65553 https://doi.org/10.7554/eLife.65553 | PubMed

55. **Singer K,** et al. (2014) Diet-induced obesity promotes myelopoiesis in hematopoietic stem cells. *Mol Metab* **3**:664-675 https://doi.org/10.1016/j.molmet.2014.06.005 | PubMed

56. **Li Z,** Hardij J, Bagchi DP, Scheller EL, MacDougald OA (2018) Development, regulation, metabolism and function of bone marrow adipose tissues. *Bone* **110**:134-140 https://doi.org/10.1016/j.bone.2018.01.008 | PubMed

57. **Tencerova M,** et al. (2018) High-Fat Diet-Induced Obesity Promotes Expansion of Bone Marrow Adipose Tissue and Impairs Skeletal Stem Cell Functions in Mice: HFD AFFECTS BM-MSC PROPERTIES AND INSULIN SENSITIVITY IN MICE. *J Bone Miner Res* **33**:1154-1165 https://doi.org/10.1002/jbmr.3408 | PubMed

58. **Campos V,** Rappaz B, Kuttler F, Turcatti G, Naveiras O (2018) High-throughput, nonperturbing quantification of lipid droplets with digital holographic microscopy. *J Lipid Res* **59**:1301-1310 https://doi.org/10.1194/jlr.d085217 | PubMed

59. **Sun H,** et al. (2013) Osteoblast-Targeted suppression of PPARγ increases osteogenesis through activation of mTOR signaling. *Stem Cells* **31**:2183-2192 https://doi.org/10.1002/stem.1455 | PubMed

60. **Cock T,** et al. (2004) Enhanced bone formation in lipodystrophic PPARγ $^{hyp/hyp}$ mice relocates haematopoiesis to the spleen. *EMBO Rep* **5**:1007-1012 https://doi.org/10.1038/sj.embor.7400254 | PubMed

61. **Li Z,** et al. (2022) Constitutive bone marrow adipocytes suppress local bone formation. *JCI Insight* **7**:e160915 https://doi.org/10.1172/jci.insight.160915 | PubMed

62. **Morowski M,** et al. (2013) Only severe thrombocytopenia results in bleeding and defective thrombus formation in mice. *Blood* **121**:4938-4947 https://doi.org/10.1182/blood-2012-10-461459 | PubMed

63. **Vannini N,** et al. (2019) The NAD-Booster Nicotinamide Riboside Potently Stimulates Hematopoiesis through Increased Mitochondrial Clearance. *Cell Stem Cell* **24**:405-418.e7 https://doi.org/10.1016/j.stem.2019.02.012 | PubMed

64. **Thompson B,** et al. (2023) Secondary bile acids function through the vitamin D receptor in myeloid progenitors to promote myelopoiesis. *Blood Adv* **7**:4970-4982 https://doi.org/10.1182/bloodadvances.2022009618 | PubMed

65. **Sorrentino G,** et al. (2020) Bile Acids Signal via TGR5 to Activate Intestinal Stem Cells and Epithelial Regeneration. *Gastroenterology* **159**:956-968.e8 https://doi.org/10.1053/j.gastro.2020.05.067 | PubMed

66. **Qi Z,** et al. (2025) The gut microbiota–bile acid–TGR5 axis orchestrates platelet activation and atherothrombosis. *Nat Cardiovasc Res* https://doi.org/10.1038/s44161-025-00637-x | PubMed

67. **Rausch P,** et al. (2016) Analysis of factors contributing to variation in the C57BL/6J fecal microbiota across German animal facilities. *Int J Med Microbiol* **306**:343-355 https://doi.org/10.1016/j.ijmm.2016.03.004 | PubMed

68. **Jaric I,** et al. (2022) The rearing environment persistently modulates mouse phenotypes from the molecular to the behavioural level. *PLOS Biol* **20**:e3001837 https://doi.org/10.1371/journal.pbio.3001837 | PubMed

69. **Ho Y.-H,** et al. (2019) Remodeling of Bone Marrow Hematopoietic Stem Cell Niches Promotes Myeloid Cell Expansion during Premature or Physiological Aging. *Cell Stem Cell* **25**:407-418.e6 https://doi.org/10.1016/j.stem.2019.06.007 | PubMed

70. **Inoue K,** et al. (2023) Bone marrow Adipoq-lineage progenitors are a major cellular source of M-CSF that dominates bone marrow macrophage development, osteoclastogenesis, and bone mass. *eLife* **12**:e82118 https://doi.org/10.7554/eLife.82118 | PubMed

71. **Rosen CJ,** Horowitz MC (2023) Nutrient regulation of bone marrow adipose tissue: skeletal implications of weight loss. *Nat Rev Endocrinol* https://doi.org/10.1038/s41574-023-00879-4 | PubMed

72. **Craft CS,** et al. (2019) Bone marrow adipose tissue does not express UCP1 during development or adrenergic-induced remodeling. *Sci Rep* **9**:17427 https://doi.org/10.1038/s41598-019-54036-x | PubMed

73. **Devlin MJ** (2011) Why does starvation make bones fat?. *Am J Hum Biol Off J Hum Biol Counc* **23**:577-585 https://doi.org/10.1002/ajhb.21202 | PubMed

74. **Devlin MJ,** et al. (2010) Caloric restriction leads to high marrow adiposity and low bone mass in growing mice. *J Bone Miner Res* **25**:2078-2088 https://doi.org/10.1002/jbmr.82 | PubMed

75. **Doucette CR,** et al. (2015) A High Fat Diet Increases Bone Marrow Adipose Tissue (MAT) But Does Not Alter Trabecular or Cortical Bone Mass in C57BL/6J Mice. *J Cell Physiol* **230**:2032-2037 https://doi.org/10.1002/jcp.24954 | PubMed

76. **Li Z,** et al. (2022) Lipolysis of bone marrow adipocytes is required to fuel bone and the marrow niche during energy deficits. *eLife* **11**:e78496 https://doi.org/10.7554/eLife.78496 | PubMed

77. **Turner RT,** Martin SA, Iwaniec UT (2018) Metabolic Coupling Between Bone Marrow Adipose Tissue and Hematopoiesis. *Curr Osteoporos Rep* **16**:95-104 https://doi.org/10.1007/s11914-018-0422-3 | PubMed

78. **Garrett J,** et al. (2019) Characterization and Etiology of Swollen Muzzles in Irradiated Mice. *Radiat Res* **191**:31-42 https://doi.org/10.1667/rr14724.1 | PubMed

79. **Gil L,** et al. (2013) Neutropenic enterocolitis after high-dose chemotherapy and autologous stem cell transplantation: incidence, risk factors, and outcome. *Transpl Infect Dis* **15**:1-7 https://doi.org/10.1111/j.1399-3062.2012.00777.x | PubMed

80. **Gooley TA,** et al. (2010) Reduced Mortality after Allogeneic Hematopoietic-Cell Transplantation. *N Engl J Med* **363**:2091-2101 https://doi.org/10.1056/nejmoa1004383 | PubMed

81. **Van De Peppel J,** et al. (2017) Identification of Three Early Phases of Cell-Fate Determination during Osteogenic and Adipogenic Differentiation by Transcription Factor Dynamics. *Stem Cell Rep* **8**:947-960 https://doi.org/10.1016/j.stemcr.2017.02.018 | PubMed

82. **Mohty M,** et al. (2020) Prophylactic, preemptive, and curative treatment for sinusoidal obstruction syndrome/veno-occlusive disease in adult patients: a position statement from an international expert group. *Bone Marrow Transplant* **55**:485-495 https://doi.org/10.1038/s41409-019-0705-z | PubMed

83. **Ueda H,** et al. (2022) Sex-, age-, and organ-dependent improvement of bile acid hydrophobicity by ursodeoxycholic acid treatment: A study using a mouse model with human-like bile acid composition. *PloS One* **17**:e0271308 https://doi.org/10.1371/journal.pone.0271308 | PubMed

84. **Heuman DM** (1989) Quantitative estimation of the hydrophilic-hydrophobic balance of mixed bile salt solutions. *J Lipid Res* **30**:719-730 https://doi.org/10.1016/s0022-2275(20)38331-0 | PubMed

85. **Shen Y,** et al. (2022) Ursodeoxycholic acid reduces antitumor immunosuppression by inducing CHIP-mediated TGF-β degradation. *Nat Commun* **13**:3419 https://doi.org/10.1038/s41467-022-31141-6 | PubMed

86. **Zhang H,** Xu H, Zhang C, Tang Q, Bi F (2021) Ursodeoxycholic acid suppresses the malignant progression of colorectal cancer through TGR5-YAP axis. *Cell Death Discov* **7**:207 https://doi.org/10.1038/s41420-021-00589-8 | PubMed

87. **Ibrahim E,** et al. (2018) Bile acids and their respective conjugates elicit different responses in neonatal cardiomyocytes: role of Gi protein, muscarinic receptors and TGR5. *Sci Rep* **8**:7110 https://doi.org/10.1038/s41598-018-25569-4 | PubMed

88. **Sepe V,** et al. (2014) Modification on ursodeoxycholic acid (UDCA) scaffold. discovery of bile acid derivatives as selective agonists of cell-surface G-protein coupled bile acid receptor 1 (GP-BAR1). *J Med Chem* **57**:7687-7701 https://doi.org/10.1021/jm500889f | PubMed

89. **Sato H,** et al. (2008) Novel potent and selective bile acid derivatives as TGR5 agonists: biological screening, structure-activity relationships, and molecular modeling studies. *J Med Chem* **51**:1831-1841 https://doi.org/10.1021/jm7015864 | PubMed

90. **Li Y.-X,** et al. (2017) Investigation of triamterene as an inhibitor of the TGR5 receptor: identification in cells and animals. *Drug Des Devel Ther* **11**:1127-1134 https://doi.org/10.2147/dddt.s131892 | PubMed

91. **Masyuk TV,** et al. (2017) TGR5 contributes to hepatic cystogenesis in rodents with polycystic liver diseases through cyclic adenosine monophosphate/Gαs signaling. *Hepatology* **66**:1197-1218 https://doi.org/10.1002/hep.29284 | PubMed

92. **Masyuk T,** et al. (2025) Targeting of a Bile Acid Receptor, Takeda G Protein Receptor 5 [TGR5], by a Novel First-in-Class Competitive Antagonist, SBI-364, Diminishes Hepatic and Renal Cystogenesis in Polycystic Liver and Kidney Disease. *ACS Pharmacol Transl Sci* **8**:1950-1964 https://doi.org/10.1021/acsptsci.4c00701 | PubMed

93. **Thirouard L,** et al. (2022) Identification of a Crosstalk among TGR5, GLIS2, and TP53 Signaling Pathways in the Control of Undifferentiated Germ Cell Homeostasis and Chemoresistance. *Adv Sci* **9**:2200626 https://doi.org/10.1002/advs.202200626 | PubMed

94. **Thomas C,** et al. (2009) TGR5-Mediated Bile Acid Sensing Controls Glucose Homeostasis. *Cell Metab* **10**:167-177 https://doi.org/10.1016/j.cmet.2009.08.001 | PubMed

95. **Bouxsein ML,** et al. (2010) Guidelines for assessment of bone microstructure in rodents using micro-computed tomography. *J Bone Miner Res* **25**:1468-1486 https://doi.org/10.1002/jbmr.141 | PubMed

96. **Maridas DE,** Rendina-Ruedy E, Le PT, Rosen CJ (2018) Isolation, Culture, and Differentiation of Bone Marrow Stromal Cells and Osteoclast Progenitors from Mice. *J Vis Exp JoVE* 56750 https://doi.org/10.3791/56750 | PubMed

Peer reviews

Reviewer #1 (Public review):

This study by Alonso-Calleja and colleagues aimed to determine whether TGR5 regulates hematopoiesis and the bone marrow microenvironment under steady-state conditions and following transplantation. The revised manuscript substantially improves upon the original submission by providing additional characterization of TGR5 expression in hematopoietic and stromal populations, incorporating analyses in female mice, and expanding the investigation of bone marrow adipose tissue under aging and high-fat diet conditions. These additions more convincingly establish TGR5 as a regulator of bone marrow adipose tissue and stromal composition.

Major strengths of the study include the comprehensive characterization of the bone marrow adipose tissue phenotype across multiple experimental settings and the demonstration that TGR5 deficiency consistently alters the stromal compartment. The strongest and most convincing aspect of the work is the identification of TGR5 as a regulator of bone marrow adipose tissue and the bone marrow microenvironment. These findings provide useful insights into how metabolic signaling pathways influence the hematopoietic niche.

However, the evidence supporting a direct role for TGR5 in hematopoietic recovery following transplantation remains limited. Although reciprocal transplantation experiments and peripheral blood recovery analyses strengthen the manuscript, the conclusions regarding hematopoietic regeneration continue to rely largely on correlative observations. The study does not directly demonstrate that expansion of adipocyte progenitors is responsible for the enhanced recovery phenotype, nor does it establish improved regeneration of hematopoietic stem or progenitor cells within the bone marrow. Overall, the revised work addresses many of the concerns raised in the original review and provides useful new insights into the regulation of the bone marrow microenvironment by TGR5. Nevertheless, the conclusions regarding hematopoietic recovery should remain appropriately tempered, as the mechanistic basis linking the stromal phenotype to enhanced regeneration has not been directly demonstrated.

https://doi.org/10.7554/eLife.93124.2.sa2

Reviewer #2 (Public review):

Summary:

The authors showed the expression of TGR5 in hematopoietic compartments and that loss of TGR5 doesn't impair steady-state hematopoiesis. Notably, TGR5 knockout significantly decreases BMAT, increase the APC population and accelerate the recovery upon bone marrow transplantation.

Strengths:

The role of TGR5 is interesting.

Weaknesses:

Additional mechanistic studies would further strengthen the work and provide deeper insight into how TGR5 regulates the bone marrow microenvironment.

https://doi.org/10.7554/eLife.93124.2.sa1

Author response:

The following is the authors' response to the original reviews

> ***eLife assessment***
>
> *This study investigates the role of the bile acid receptor TGR5 in adult hematopoiesis of the mouse model. The findings are potentially useful because the loss of TGR5 leads to dysregulation of bone marrow adipose tissue (BMAT) that has emerging regulatory functions. However, the study is still incomplete because the mechanism of TGR5 is not clear, the stromal cells expressing TGR5 have not been well defined, and there is not strong evidence for the role of TGR5 in recovery from transplant stress.*

We thank the eLife editorial team for handling our manuscript. In our revised version, we took into consideration the suggestions of the reviewers, which we believe have significantly improved the quality of the current study. In summary, our new data provide further evidence that TGR5 is expressed in both hematopoietic cell lineage and stromal cells of the bone marrow (BM), including subpopulation analyses for both. While steady-state hematopoiesis remains intact in TGR5 knockout mice, we demonstrate that loss of TGR5 significantly impacts progenitor reconstitution under stress conditions, alters the BM adipose tissue (BMAT) homeostasis in a sex-specific manner and influences the balance of stromal cell differentiation. In particular, TGR5 deficiency resulted in reduced regulated BMAT and an accumulation of adipocyte progenitors, correlating with improved hematopoietic recovery following BM transplantation. The BMAT decrease is further observed in physiologically and pathophysiologically relevant contexts such as aging and obesity, where TGR5 deficiency is associated with a decrease in the myeloid bias. Collectively, our findings support a previously unrecognized role for TGR5 in maintaining BM niche integrity and highlight its potential as a modulator of hematopoietic support, although the precise molecular mechanisms still need to be elucidated.

> ***Public Reviews:***
>
> ***Reviewer #1 (Public Review):***
>
> *Summary:*
>
> *Alonso-Calleja and colleagues explore the role of TGR5 in adult hematopoiesis at both steady state and post-transplantation. The authors utilize two different mouse models including a TGR5-GFP reporter mouse to analyze the expression of TGR5 in various hematopoietic cell subsets. Using germline Tgr5-/- mice it's reported that loss of Tgr5 has no significant impact on steady-state hematopoiesis, with a small decrease in trabecular bone fraction, associated with a reduction in proximal tibia adipose tissue, and an*

> *increase in marrow phenotypic adipocytic precursors. The authors further explored the role of stroma TGR5 expression in the hematopoietic recovery upon bone marrow transplantation of wild-type cells, although the studies supporting this claim are weak. Overall, while most of the hematopoietic phenotypes have negative results or small effects, the role of TGR5 in adipose tissue regulation is interesting to the field.*
>
> *Strengths:*
>
> *This is the first time the role of TGR5 has been examined in the bone marrow.*
>
> *This paper supports further exploration of the role of bile acids in bone marrow transplantation and possible therapeutic strategies.*

We thank the reviewer for pinpointing the strengths of our study.

> *Weaknesses:*
>
> *(1) The authors fail to describe whether niche stroma cells or adipocyte progenitor cells (APCs) express TGR5.*

Using the TGR5:GFP reporter model, we identified GFP^+ cells in the stroma-enriched CD45-Ter119-CD31- population that contains the adipogenic progenitor cells (APC).

These data, along with the corresponding gating strategy are outline in Figure 6A and B.

We found the subpopulation analyses within the stroma gate challenging at the individual mouse level given the limited cell numbers for these progenitor populations. We attempted to circumvent this by concatenating the individual files per genotype (WT and TGR5:GFP) for two independent experiments. We were surprised to find that there is little to no GFP expression in the APC population. Nevertheless, we found that the $CD45^-Ter119^-CD31^-CD24^+Sca1+$, multi-potent stem cell-like population (Ambrosi et al., 2017), reproducibly showed a TGR5:GFP positivity comparable to that of $Ly6^{lo}$ monocytes. We believe this would be compatible with our results showing an increase in CFU-F in *Tgr5*$^{-/-}$ mice, but we remain cautious about its interpretation. Results are shown in Author response image 1 for the concatenated flow plots and numerically in Error! Reference source not found. considering all individual mice analyzed (i.e., non pooled) for completeness. We kindly request the Reviewer's opinion on whether these subpopulation analyses should be included in the main manuscript or solely here as part of the public review section.

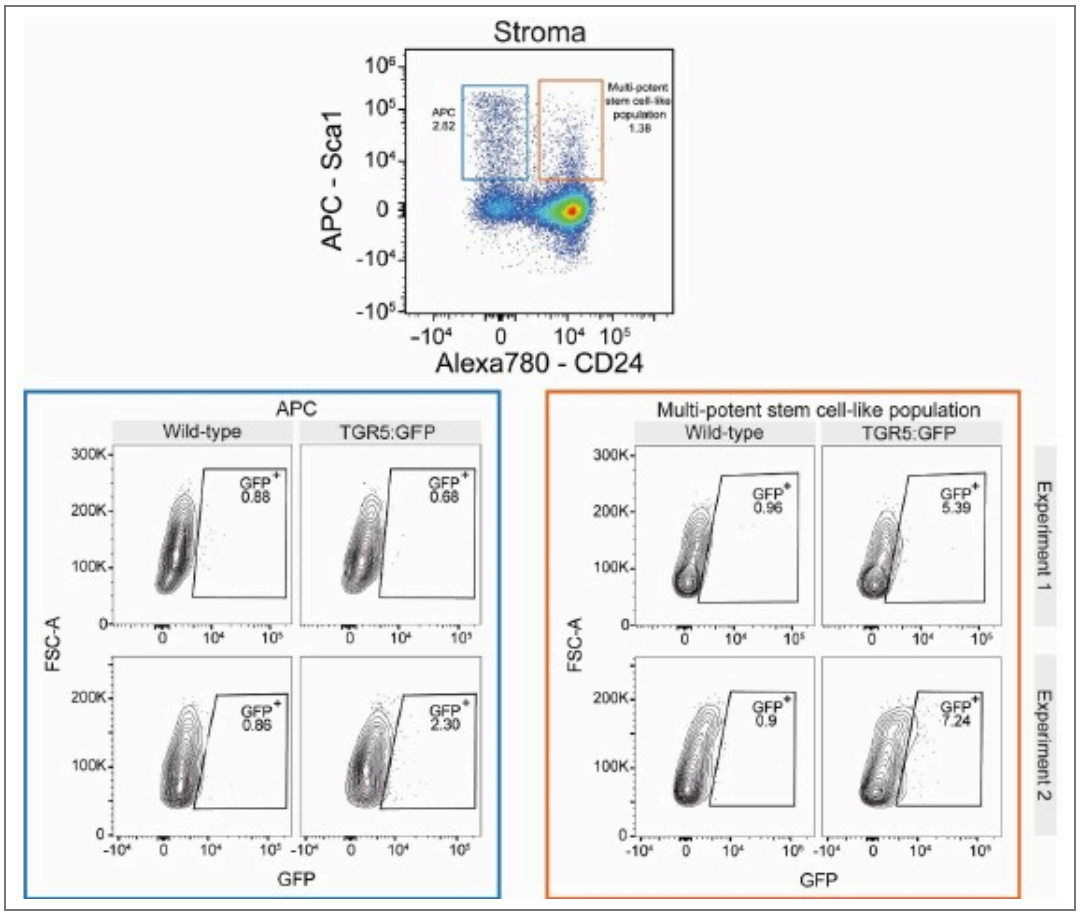

Author response image 1. Flow cytometry gating strategy used to identify stroma subpopulations in the stroma enriched CD45$^-$Ter119$^-$CD31$^-$ gate and their GFP signal for BM cells in TGR5:GFP mice. Subpopulations were immunophenotypically defined as CD45$^-$Ter119$^-$CD31$^-$CD24$^+$Sca1+ (adipogenic progenitor cells (APC)) and CD45Ter119$^-$CD31$^-$CD24$^+$Sca1+ (multi-potent stem cell-like populations) (Ambrosi et al., 2017). Results are shown as the concatenated data of all mice in each phenotype for two independent experiments, as indicated.

	APC		Multi-potent stem cell-like population	
Experiment (mice per exp.)	**Wild-type (n=3,5)**	**TGR5:GFP (n=4,4)**	**Wild-type (n=3,5)**	**TGR5:GFP (n=4,4)**
1 (Avg +/- 95% CI)	0.21 +/- 0.55%	1.63 +/- 0.91	1.22 +/- 1.23	7.59 +/- 6.29 **
2(Avg, +/- 95% CI)	0.79 +/- 0.41%	0.73 +/- 0.48	0.97 +/- 0.33	5.23 +/- 3.63 **

Author response table 1. Frequencies in the total live cell gate for adipogenic progenitor cells (APC) and CD45Ter119$^-$CD31$^-$CD24$^+$Sca1+ (multi-potent stem cell-like populations, MPSC-like) (gating as in Ambrosi et al. , 2017) in the experiments presented in Author Response Figure 1, expressed as average +/- 95% confidence interval for the two independent experiments. The number of mice per genotype and per experiment is indicated in parenthesis. **Paired, two-tailed Student's t-test statistical analysis for the combined experiments (n=8 per group) indicates $p < 0.01$ for GFP expressing cells in APC versus MPSC-like populations.

> *(2) Although the authors note a significant reduction in bone marrow adipose tissue in Tgr5-/- mice, they do not address whether this is white or brown adipose tissue especially since BA-TGR5 signaling has been shown to play a role in beiging.*

The nature of BMAT and how it relates to brown, white or brown/beige adipose tissue has been a persisting question in the field. Our understanding is that BMAT is currently considered as a distinct adipose depot that is neither white nor brown/beige (Sebo et al., 2019; Suchacki et al., 2020). BMAT does not express UCP1 to an appreciable extent, with reports showing that detectable expression possibly stems from contamination by tissues surrounding bone (Craft et al., 2019). Beyond this consideration, as the regulated BMAT in *Tgr5*$^{-/-}$ mice is almost absent, determination of the brown/beige vs white nature of the little regulated BMAT that remains would be technically extremely challenging.

> *(3) In Figure 1, the authors explore different progenitor subsets but stop short of describing whether TGR5 is expressed in hematopoietic stem cells (HSCs).*

We have added these data to the manuscript as part of Figure 1C.

We have further expanded our data in Figure 1D and Figure 1–figure supplement 1A with the expression of TGR5:GFP in megakaryocyte progenitors (Lin$^-$cKit$^+$Sca1CD150$^+$CD41$^+$) as shown in Author response image 2.

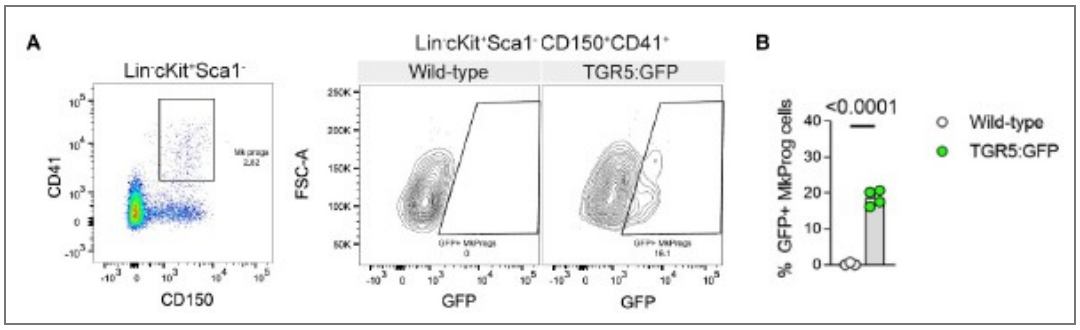

Author response image 2. A, representative flow cytometry gating strategy used to identify megakaryocyte progenitors (MkProg) and GFP positivity in TGR5:GFP mice and their wild-type controls. B, frequencies of GFP$^+$ cells in MkProg population in the BM of 8-12-week-old male TGR5:GFP mice and their controls (n=3 for wild-type control mice, n=4 for TGR5:GFP mice). Results represent the mean ± s.e.m., n represents biologically independent replicates. Two-tailed Student's t-test (B) was used for statistical analysis. p-values (exact value) are indicated.

Finally, we have completed the characterization of BM progenitor populations to include the erythroid lineage, thus covering the main hematopoietic populations. We have added these data to Figure 1E and Figure 1–figure supplement 1B.

> *(4) Are there more CD45+ cells in the BM because hematopoietic cells are proliferating more due to a direct effect of the loss of Tgr5 or is it because there is just more space due to less trabecular bone?*

We observe an average 20% increase in CD45$^+$ cell counts in baseline *Tgr5*$^{-/-}$ mice. The absolute volume of bone and BMAT lost in these animals does not account for 20% of the medullary cavity volume, so we speculate that the increase in CD45$^+$ counts is not solely due to increased available volume for these cells.

> *(5) In Figure 4 no absolute cell counts are provided to support the increase in immunophenotypic APCs (CD45-Ter119-CD31-Sca1+CD24-) in the stroma of Tgr5-/- mice. Accordingly, the absolute number of total stromal cells and other stroma niche cells such as MSCs, ECs are missing.*

These data are now included in the manuscript and in Author response image 3. Although we detect an increase in the relative frequency of APCs (Figure 7A), on a per-leg basis we did not

detect an increase in APC numbers per leg (Author response image 3). We did however observe a decrease in total CD45⁻Ter119sup>-CD31sup>- stromal-enriched cells in *Tgr5*-/- mice. Nevertheless, given that only 2–5% of stromal cells are recovered in single-cell suspensions compared with native tissue (Coutu et al., 2017; Gomariz et al., 2018), we consider results for absolute stromal cell numbers prone to over interpretation. Our conclusion, therefore, remains one of relative enrichment of immunophenotypic APCs, supported by *in vitro* findings of increased adipogenesis and CFU-F formation after plating equal cell numbers.

Endothelial cells (CD45⁻Ter119⁻CD31⁺) were also quantified, with no differences observed between groups.

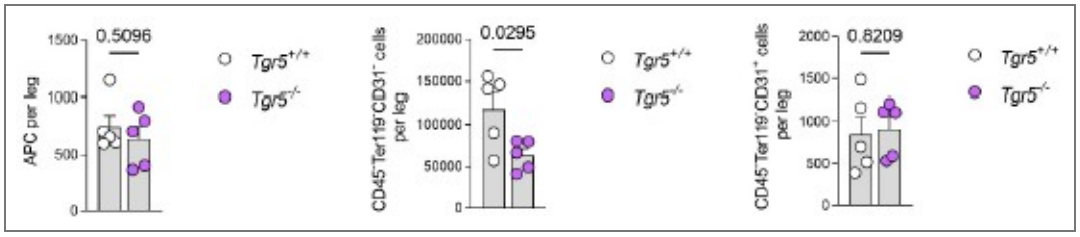

Author response image 3. Absolute number of adipocyte progenitor cells (APC), stroma cells (CD45-Ter119CD31⁻) and endothelial cells (CD45⁻Ter119⁻CD31⁺) (n=5 for both *Tgr5*$^{+/+}$ and *Tgr5*$^{-/-}$ mice). Results represent the mean ± s.e.m., n represents biologically independent replicates. Unpaired, two-tailed Student's t-test was used for statistical analysis. p values (exact values) are shown.

> *(6) There are issues with the reciprocal transplantation design in Fig 4. Why did the authors choose such a low dose (250 000) of BM cells to transplant? If the effect is true and relevant, the early recovery would be observed independently of the setup and a more robust engraftment dataset would be observed without having lethality post-transplant. On the same note, it's surprising that the authors report ~70% lethality post-transplant from wild-type control mice (Fig 4E), according to the literature 200 000 BM cells should ensure the survival of the recipient post-TBI. Overall, the results even in such a stringent setup still show minimal differences and the study lacks further in-depth analyses to support the main claim.*

We thank the reviewer for this comment. On the one hand, we respectfully disagree on the relevance of the effect size, as *Tgr5*$^{-/-}$ mice recover from low platelet and leukocyte counts significantly faster than wild-type controls. *Tgr5*$^{-/-}$ recipients recovered their platelet levels faster than the *Tgr5*$^{+/+}$ recipients, showing values consistently above 200.000/µL one week sooner; platelet levels below this threshold are considered a risk factor for bleeding events (Morowski et al., 2013; Vannini et al., 2019). In addition, on day 15 post-irradiation, *Tgr5*$^{-/-}$ recipients had higher neutrophil levels, at over the 500 cells/µL-threshold value for infection risk (Morowski et al., 2013; Vannini et al., 2019), but this difference was no longer statistically significant upon stringent multiple-comparison correction (uncorrected p-value 0.028, multiplecomparison corrected p-value 0.108). Underlining the relevance, in a clinical setting, G-CSF is routinely administered to patients daily to enhance myeloid recovery even if the acceleration of recovery is by 1-2 days (Trivedi et al., 2009).

From the perspective of mortality, we agree that it is higher than expected and constitutes a limitation of our work. Note that we discovered a mistake in data plotting during the preparation of the revised version of the manuscript which renders the mortality curve no longer statistically significant, with a *p* value that changed from 0.0254 to 0.0676. We have duly changed our interpretation in the text to that of a trend towards higher survival.

Regarding the mortality in our experiments being higher than expected, we have unfortunately suffered from cases of "swollen muzzles syndrome" in our facilities that have greatly hampered our ability to perform myeloablation experiments (Garrett et al., 2018), as even sublethal doses have resulted in the appearance of side effects that were reasons for euthanasia under Swiss legislation. For example, a strong reduction in mobility requires immediate euthanasia. All experiments were performed blinded to genotype allocation, so we can reasonably exclude experimenter bias. Finally, it could be argued that mice with more marked symptomatology leading to euthanasia are more likely to have hematopoietic deficits, which in our case was mostly seen for WT animals. We have therefore chosen to report mortality alongside the longitudinal assessment of peripheral blood counts to ensure clarity of the coherent effect and full transparency. We strongly believe that this disclosure, when examined as a limitation in the discussion section, aligns with the open science efforts advocated by eLife. Unfortunately, it is beyond the scope of this manuscript and the authors' timeline to rederive the *Tgr5*$^{-/-}$ colony in our new facility and perform new bone marrow transplantation studies with titrating doses of BM.

Lastly, the choice of 250,000 BM cells serves as the control dose per recommended standards for competitive repopulation assays (Purton and Scadden, 2007). Quoting from this methodological reference paper: "In our experiments, each recipient mouse receives cell doses … together with 2x10^5 competing congenic bone marrow. We have found these cell doses sufficient to detect both reductions (Purton et al., 2006) and increases (Janzen et al., 2006; Walkley et al., 2005) in HSC numbers in different mutant mice… Furthermore, caution should be used when designing competitive repopulation assays, as it has been shown that the reliability of this assay is critically dependent on the numbers of HSCs present in the populations being assessed: when too few or too many HSCs (recipients of <1 1x10^5 or >2x10^7 bone marrow cells each from donor and competing sources) are present, the data may not be meaningful (Harrison et al., 1993)."

Moreover, our lethal radiation rescue experiments with 2.5x105 cells are designed to deliver a minimal hematopoietic source known to rescue the great majority of animals in standard conditions, and thus to best mimic the situations when enhancement of hematopoietic recovery would be clinically meaningful (as used by our group members in (Naveiras et al., 2009; Tratwal et al., 2020; Vannini et al., 2019)). In our hands and in the absence of "swollen muzzles syndrome", this approach leads to 80-95% overall survival, which mirrors the clinical setting of autologous transplantation that our transplants are meant to mimic. In clinical practice strategies, enhancing hematopoietic recovery would be most useful to improve morbimortality in either alternative hematopoietic progenitor allotransplants, known associated with delayed engraftment, or in the case of febrile neutropenia associated to bacteriemia, which affects 11-15% of both hematopoietic autologous or allogeneic transplant patients (Gil et al., 2013; Gooley et al., 2010). In summary, septic neutropenia was unfortunately modelled by the rescue experiments presented in Figure 7 C-J with swollen muzzles syndrome concomitant to the reconstitution, but we strongly believe that this complication enhances the clinical relevance of our data.

> *(7) Mechanistically, how does the loss of Tgr5 impact hematopoietic regeneration following sublethal irradiation?*

As delineated in the previous point, we have been seriously conditioned by cases of "swollen muzzles syndrome" (Garrett et al., 2018), which has stopped us from proceeding with more irradiation experiments for this particular study. Mechanistic studies are unfortunately beyond the scope of this manuscript, but the mechanistic basis for the relationship between BM adipocyte differentiation and hematopoiesis is now a focus for one of the involved laboratories and should produce follow-up manuscripts in the near future.

> *(8) Only male mice were used throughout this study. It would be beneficial to know whether female mice show similar results.*

We thank Reviewer #1 for this question, as it led us to perform the characterization of steady-state hematopoiesis and morphological bone and BMAT evaluation of young female mice, yielding new findings that strengthen our manuscript. In summary, we have found that the decrease in BMAT is sexually dimorphic, with young females not showing reduced BMAT levels. Conversely, we did find a trend towards lower trabecular bone content in females. We present these data as part of Figure 3.

> ***Reviewer #2 (Public Review):***
>
> *Summary:*
>
> *In this manuscript, the authors examined the role of the bile acid receptor TGR5 in the bone marrow under steady-state and stress hematopoiesis. They initially showed the expression of TGR5 in hematopoietic compartments and that loss of TGR5 doesn't impair steady-state hematopoiesis. They further demonstrated that TGR5 knockout significantly decreases BMAT, increases the APC population, and accelerates the recovery upon bone marrow transplantation.*
>
> *Strengths:*
>
> *The manuscript is well-structured and well-written.*

We thank Reviewer #2 for this comment.

> *Weaknesses:*
>
> *The mechanism is not clear, and additional studies need to be performed to support the authors' conclusion.*

We agree with Reviewer #2 that more studies are needed to understand the role of TGR5 in the hematopoietic system. We have been hampered in our studies of stress hematopoiesis because of frequent cases of swollen muzzles syndrome (Garrett et al., 2018), which prevented us from conducting additional experiments involving myelosuppression. Furthermore, the identification of the mechanism that links changes in the adipocyte differentiation axis and hematopoietic support, which is more complex than initially thought, has become a top priority for one of the involved laboratories and should produce follow-up manuscripts in the near future.

> ***Recommendations For The Authors:***
>
> ***Reviewer #2 (Recommendations For The Authors):***
>
> *(1) Figure 1: the authors showed the presence of TGR5 in hematopoietic cells using a GFP report in mice. What's the expression pattern of TGR5 in the nonhematopoietic cells? For example, adipocytes, stromal cells, endothelial cells, etc. In addition to analyze the percentage of TGR5-GFP+ cells, the authors should also quantify the expression levels of TGR5 in various hematopoietic and niche components.*

We thank Reviewer #2 for this question, which we have addressed as points 1 and 3 from Reviewer #1. The expression of TGR5:GFP signal in stromal cells, HSCs, and the various hematopoietic compartments is now presented respectively as new panels in Figure 6A-B, Figure 1C-D, Figure 1–Figure Supplement 1A-B, and Figure 1figure supplement 2A, as well as Author response image 1 for stromal progenitors. Please note that specifically for the stromal compartment, we kindly requested Reviewer #1's opinion on whether these subpopulation analyses should be included in the main manuscript or solely here as part of the public

review section, as we are concerned about over interpretation for these rare APC and multi-potent stem cell-like subpopulations.

Consistent with the typical low-abundance expression of G protein-coupled receptors, where ligand-mediated activation is more relevant than absolute receptor abundance, TGR5 is also lowly expressed in most cell types. Although technical limitations prevent us from directly quantifying TGR5 expression in adipocytes (due to the difficulty of isolating these populations from bone marrow), previous studies have reported TGR5 expression in human BMSC-derived adipocytes (Velazquez-Villegas et al., 2018) . For similar reasons, we could not quantify TGR5 expression levels by RT-qPCR in the bone marrow niche, as isolating enough cells from each compartment to reliably detect a low-abundance receptor is technically challenging.

Regarding endothelial cells, previous studies have shown TGR5 expression in vascular endothelial cells (Kida et al., 2013) as well. In our dataset the number of endothelial cells recovered was limited, largely due to the lack of a dedicated endothelial isolation protocol for the BM. Even so, the data we collected are shown as Author response image 4 and Author response table 2 and suggest that TGR5:GFP level in endothelial cells is lower than in the stromal and hematopoietic compartments. As for Author response image 1 and Author response table 1, we remain cautious about the interpretation of GFP expression in these low frequency stromal and endothelial populations and we kindly request the Reviewer's opinion on whether these subpopulation analyses should be included in the main manuscript or solely here as part of the public review section.

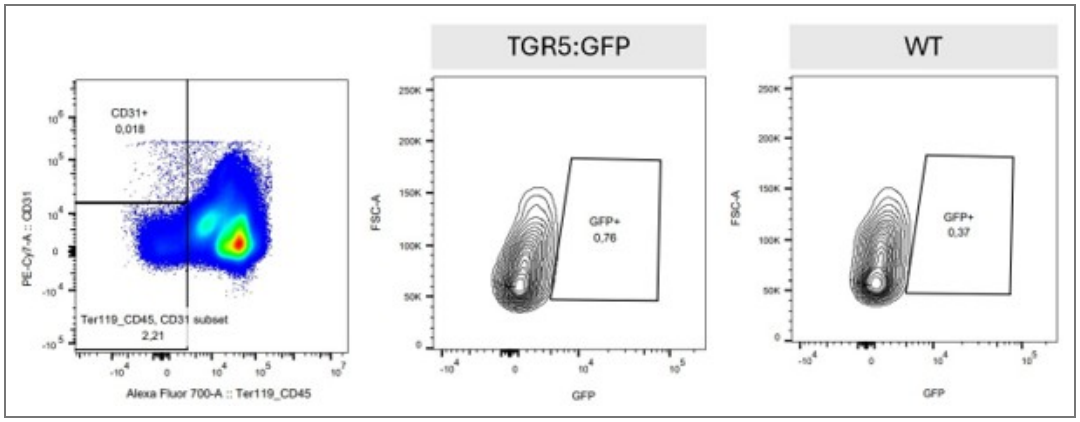

Author response image 4. Representative flow cytometry gating strategy used to identify endothelial cells in BM, defined as CD45$^-$Ter119$^-$CD31$^+$ and their GFP positivity in TGR5:GFP mice.

	Experiment 1 (mice per exp.)		Experiment 2 (mice per exp.)	
	Wild-type (n=3)	**TGR5:GFP (n=4)**	**Wild-type (n=5)**	**TGR5:GFP (n=5)**
Avg (StD)	0,76% (1%)	0,76% (1%)	3,71% (5%)	0,64% (1%)

Author response table 2. Frequency of GFP-expressing cells in the CD45$^-$Ter119$^-$CD31$^+$ gate for endothelial cells presented in Author Response Figure 4, expressed as average (standard deviation). The number of mice per genotype and per experiment is indicated in parenthesis.

> *(2) Figure 2: Regarding the competitive transplantation, the authors should bleed the mice every 4 weeks and show the dynamics of donor chimerism up to 16 or 20 weeks. The difference at the 3-week time point is very tiny and is this change significant? There is no statistical significance shown in Supplemental Figure 2 Panel C at a 3-week time point.*

The full data for repetitive monthly bleedings in primary, secondary and tertiary transplants is now shown in Figure 2J and Figure 2-figure supplement 1I-K. The statistically significant difference on the first month, which represents a 26% loss in short-time progenitor phenotype, is small but potentially clinically relevant as it is these progenitors that sustain early hematopoietic recovery from severe leucopenia and thrombocytopenia. Indeed, the hematopoietic phenotype described in Figure 7 C-J for accelerated rescue of *Tgr5*$^{-/-}$ recipients with wild-type bone marrow would be coherently associated to this short-term progenitor phenotype.

> *(3) Figure 3: in addition to the irradiation/transplantation model, the authors should also use alternative models for stress hematopoietic, for example, 5-FU, etc.*

This is an excellent suggestion, but unfortunately beyond the scope of this manuscript due to the move of one of the co-senior authors to another institution. Follow-up studies are however planned with ablative chemotherapy models relevant to the hematopoietic transplant setting (non 5-FU).

> *(4) To get a better understanding of the role of TGR5 in the bone marrow niche, the authors should get and/or generate the TGR5 floxed mice and this will allow the authors to delete it from specific cell populations using cell-type specific Cre. In addition, it would be very interesting to investigate further the molecular mechanisms downstream of TGR5.*

We much appreciate this comment and the interest it reflects in TGR5 BM biology. Mechanistic studies are unfortunately beyond the scope of this manuscript, but the mechanistic basis for the relationship between BM adipocyte differentiation and hematopoiesis are now a focus for one of the involved laboratories and should produce concrete follow-up manuscripts soon.

References

Ambrosi, T.H., Scialdone, A., Graja, A., Gohlke, S., Jank, A.-M., Bocian, C., Woelk, L., Fan, H., Logan, D.W., Schürmann, A., Saraiva, L.R., Schulz, T.J., 2017. Adipocyte Accumulation in the Bone Marrow during Obesity and Aging Impairs Stem Cell-Based Hematopoietic and Bone Regeneration. Cell Stem Cell 20, 771-784.e6. *https://doi.org/10.1016/j.stem.2017.02.009*

Coutu, D.L., Kokkaliaris, K.D., Kunz, L., Schroeder, T., 2017. Three-dimensional map of nonhematopoietic bone and bone-marrow cells and molecules. Nat Biotechnol 35, 1202–1210. *https://doi.org/10.1038/nbt.4006*

Craft, C.S., Robles, H., Lorenz, M.R., Hilker, E.D., Magee, K.L., Andersen, T.L., Cawthorn, W.P., MacDougald, O.A., Harris, C.A., Scheller, E.L., 2019. Bone marrow adipose tissue does not express UCP1 during development or adrenergic-induced remodeling. Sci Rep 9, 17427. *https://doi.org/10.1038/s41598-019-54036-x*

Garrett, J., Sampson, C.H., Plett, P.A., Crisler, R., Parker, J., Venezia, R., Chua, H.L., Hickman, D.L., Booth, C., MacVittie, T., Orschella, C.M., Dynlachta, J.R., 2018. Characterization and Etiology of Swollen Muzzles in Irradiated Mice. Radiation Research 191, 31. *https://doi.org/10.1667/RR14724.1*

Gil, L., Poplawski, D., Mol, A., Nowicki, A., Schneider, A., Komarnicki, M., 2013. Neutropenic enterocolitis after high-dose chemotherapy and autologous stem cell transplantation:

incidence, risk factors, and outcome. Transpl Infect Dis 15, 1–7. *https://doi.org/10.1111/j.1399-3062.2012.00777.x*

Gomariz, A., Helbling, P.M., Isringhausen, S., Suessbier, U., Becker, A., Boss, A., Nagasawa, T., Paul, G., Goksel, O., Székely, G., Stoma, S., Nørrelykke, S.F., Manz, M.G., Nombela-Arrieta, C., 2018. Quantitative spatial analysis of haematopoiesis-regulating stromal cells in the bone marrow microenvironment by 3D microscopy. Nat Commun 9, 2532. *https://doi.org/10.1038/s41467-018-04770-z*

Gooley, T.A., Chien, J.W., Pergam, S.A., Hingorani, S., Sorror, M.L., Boeckh, M., Martin, P.J., Sandmaier, B.M., Marr, K.A., Appelbaum, F.R., Storb, R., McDonald, G.B., 2010. Reduced mortality after allogeneic hematopoietic-cell transplantation. N Engl J Med 363, 2091–2101. *https://doi.org/10.1056/NEJMoa1004383*

Harrison, D.E., Jordan, C.T., Zhong, R.K., Astle, C.M., 1993. Primitive hemopoietic stem cells: direct assay of most productive populations by competitive repopulation with simple binomial, correlation and covariance calculations. Exp Hematol 21, 206–219.

Janzen, V., Forkert, R., Fleming, H.E., Saito, Y., Waring, M.T., Dombkowski, D.M., Cheng, T., DePinho, R.A., Sharpless, N.E., Scadden, D.T., 2006. Stem-cell ageing modified by the cyclin-dependent kinase inhibitor p16INK4a. Nature 443, 421–426. *https://doi.org/10.1038/nature05159*

Kida, T., Tsubosaka, Y., Hori, M., Ozaki, H., Murata, T., 2013. Bile acid receptor TGR5 agonism induces NO production and reduces monocyte adhesion in vascular endothelial cells. Arterioscler Thromb Vasc Biol 33, 1663–1669. *https://doi.org/10.1161/ATVBAHA.113.301565*

Morowski, M., Vögtle, T., Kraft, P., Kleinschnitz, C., Stoll, G., Nieswandt, B., 2013. Only severe thrombocytopenia results in bleeding and defective thrombus formation in mice. Blood 121, 4938–4947. *https://doi.org/10.1182/blood-2012-10-461459*

Naveiras, O., Nardi, V., Wenzel, P.L., Hauschka, P.V., Fahey, F., Daley, G.Q., 2009. Bonemarrow adipocytes as negative regulators of the haematopoietic microenvironment. Nature 460, 259–263. *https://doi.org/10.1038/nature08099*

Purton, L.E., Dworkin, S., Olsen, G.H., Walkley, C.R., Fabb, S.A., Collins, S.J., Chambon, P., 2006. RARgamma is critical for maintaining a balance between hematopoietic stem cell self-renewal and differentiation. J Exp Med 203, 1283–1293. *https://doi.org/10.1084/jem.20052105*

Purton, L.E., Scadden, D.T., 2007. Limiting factors in murine hematopoietic stem cell assays. Cell Stem Cell 1, 263–270. *https://doi.org/10.1016/j.stem.2007.08.016*

Sebo, Z.L., Rendina-Ruedy, E., Ables, G.P., Lindskog, D.M., Rodeheffer, M.S., Fazeli, P.K., Horowitz, M.C., 2019. Bone Marrow Adiposity: Basic and Clinical Implications. Endocr Rev 40, 1187–1206. *https://doi.org/10.1210/er.2018-00138*

Suchacki, K.J., Tavares, A.A.S., Mattiucci, D., Scheller, E.L., Papanastasiou, G., Gray, C., Sinton, M.C., Ramage, L.E., McDougald, W.A., Lovdel, A., Sulston, R.J., Thomas, B.J., Nicholson, B.M., Drake, A.J., Alcaide-Corral, C.J., Said, D., Poloni, A., Cinti, S., Macpherson, G.J., Dweck, M.R., Andrews, J.P.M., Williams, M.C., Wallace, R.J., Van Beek, E.J.R., MacDougald, O.A., Morton, N.M., Stimson, R.H., Cawthorn, W.P., 2020. Bone marrow adipose tissue is a unique adipose subtype with distinct roles in glucose homeostasis. Nat Commun 11, 3097. *https://doi.org/10.1038/s41467-020-16878-2*

Tratwal, J., Bekri, D., Boussema, C., Sarkis, R., Kunz, N., Koliqi, T., Rojas-Sutterlin, S., Schyrr, F., Tavakol, D.N., Campos, V., Scheller, E.L., Sarro, R., Bárcena, C., Bisig, B., Nardi, V., de Leval, L., Burri, O., Naveiras, O., 2020. MarrowQuant Across Aging and Aplasia: A Digital Pathology

Workflow for Quantification of Bone Marrow Compartments in Histological Sections. Front Endocrinol (Lausanne) 11, 480. *https://doi.org/10.3389/fendo.2020.00480*

Trivedi, M., Martinez, S., Corringham, S., Medley, K., Ball, E.D., 2009. Optimal use of G-CSF administration after hematopoietic SCT. Bone Marrow Transplant 43, 895–908. *https://doi.org/10.1038/bmt.2009.75*

Vannini, N., Campos, V., Girotra, M., Trachsel, V., Rojas-Sutterlin, S., Tratwal, J., Ragusa, S., Stefanidis, E., Ryu, D., Rainer, P.Y., Nikitin, G., Giger, S., Li, T.Y., Semilietof, A., Oggier, A., Yersin, Y., Tauzin, L., Pirinen, E., Cheng, W.-C., Ratajczak, J., Canto, C., Ehrbar, M., Sizzano, F., Petrova, T.V., Vanhecke, D., Zhang, L., Romero, P., Nahimana, A., Cherix, S., Duchosal, M.A., Ho, P.-C., Deplancke, B., Coukos, G., Auwerx, J., Lutolf, M.P., Naveiras, O., 2019. The NAD-Booster Nicotinamide Riboside Potently Stimulates Hematopoiesis through Increased Mitochondrial Clearance. Cell Stem Cell 24, 405-418.e7. *https://doi.org/10.1016/j.stem.2019.02.012*

Velazquez-Villegas, L.A., Perino, A., Lemos, V., Zietak, M., Nomura, M., Pols, T.W.H., Schoonjans, K., 2018. TGR5 signalling promotes mitochondrial fission and beige remodelling of white adipose tissue. Nat Commun 9, 245. *https://doi.org/10.1038/s41467-017-02068-0*

Walkley, C.R., Fero, M.L., Chien, W.-M., Purton, L.E., McArthur, G.A., 2005. Negative cellcycle regulators cooperatively control self-renewal and differentiation of haematopoietic stem cells. Nat Cell Biol 7, 172–178. *https://doi.org/10.1038/ncb1214*

https://doi.org/10.7554/eLife.93124.2.sa0